

Assimilation of citizen science data in snowpack modeling using a new snow dataset: Community Snow Observations

Ryan L. Crumley^{1,2}, David F. Hill³, Katreen Wikstrom Jones⁴, Gabriel J. Wolken^{4,5}, Anthony A. Arendt⁶, Christina M. Aragon¹, Christopher Cosgrove⁷, Community Snow Observations Participants⁸

¹Water Resources Science, Oregon State University, Corvallis, OR 97331, USA

²Earth and Environmental Sciences, Los Alamos National Laboratory, Los Alamos, NM 87545, USA

³School of Civil and Construction Engineering, Oregon State University, Corvallis, OR 97331, USA

⁴Alaska Division of Geological and Geophysical Surveys, Fairbanks, AK 99709, USA

⁵International Arctic Research Center, University of Alaska Fairbanks, Fairbanks, AK 99775, USA

⁶University of Washington, Applied Physics Laboratory, WA 98105, USA

⁷Geography Department, Oregon State University, Corvallis, OR 97331, USA

⁸Citizen scientists participating in the project Community Snow Observations (CSO)

Correspondence to: Ryan L. Crumley (ryanlcrumley@gmail.com)

Abstract.

A physically-based snowpack evolution and redistribution model was used to test the effectiveness of assimilating crowd-sourced snow depth measurements collected by citizen scientists. The Community Snow Observations (CSO; communitysnowobs.org) project gathers, stores, and distributes measurements of snow depth recorded by recreational users and snow professionals in high mountain environments. These citizen science measurements are valuable since they come from terrain that is relatively under-sampled and can offer *in-situ* snow information in locations where snow information is sparse or non-existent. The present study investigates 1) the improvements to model performance when citizen science measurements are assimilated and 2) the number of measurements necessary to obtain those improvements. Model performance is assessed by comparing time series of observed (snow pillow) and modeled snow water equivalent values, by comparing spatially-distributed maps of observed (remotely sensed) and modeled snow depth, and by comparing fieldwork results from within the study area. The results demonstrate that few citizen science measurements are needed to obtain improvements in model performance and these improvements are found in 62% to 78% of the ensemble simulations, depending on the model year. Model estimations of total water volume from a sub-region of the study area also demonstrate improvements in accuracy after CSO measurements have been assimilated. These results suggest that even modest measurement efforts by citizen scientists have the potential to improve efforts to model snowpack processes in high mountain environments, with implications for water resource management and process-based snow modeling.

1 Introduction

The importance of snow in ecosystem function, in both human and natural systems, and in water resource management in western North America cannot be overstated (Bales et al., 2006; Mankin et al., 2015; Viviroli et al., 2007). Internationally, more than a billion people live in watersheds where snow is an integral part of the hydrologic system (Barnett et al., 2005). Snowpack dynamics

41 in mountainous, headwater catchments play an essential role connecting atmospheric processes and the hydrologic cycle with
42 downstream water users, agricultural systems, and municipal water systems (Fayad et al., 2017; Holko et al., 2011; Schneider et
43 al., 2013).

44
45 Information about snow distribution comes from many sources. First, there are snow datasets in the form of *in-situ* observations
46 of snowpack conditions, often observations of snow depth or snow water equivalent (SWE). In the United States of America (U.S.),
47 snow depth and SWE data are collected by the National Resources Conservation Service's (NRCS) Snow Telemetry (SNOTEL)
48 network using snow pillows and snow courses. Similar national *in-situ* snow observational networks exist in Europe, like the
49 MeteoSwiss and MeteoFrance programs that include snow depth, snowfall, and SWE datasets. For a comprehensive overview of
50 snow observations in Europe, including each program name, the location of observations, and agency websites, see the European
51 Snow Booklet (Haberkorn, 2019). Snow course information is also collected by state programs such as the California Cooperative
52 Snow Survey in the U.S. and, in the case of Canada, by provincial programs such as the British Columbia Snow Survey. These *in-*
53 *situ* snow observations provide critical information on snow conditions and snow distribution worldwide, but vast areas of
54 snowpack remain unsampled.

55
56 To fill the observational gaps associated with point measurements, we often turn to snow information in the form of remote sensing
57 (RS) datasets, like the NASA-based Airborne Snow Observatory (Painter et al., 2016) that uses aerial light detection and ranging
58 (LiDAR) in catchment-scale study areas. Other catchment-scale snow RS datasets are collected using unmanned aerial systems,
59 including high-elevation capable drones and balloon-based platforms in conjunction with structure-from-motion photogrammetry
60 (Bühler et al., 2016; Li et al., 2019). There are also RS datasets covering hemispheric and global scales, like the daily snow-covered
61 area product from the MODIS satellite or the GlobSnow snow extent product from the European Space Agency (Hall and Riggs,
62 2016; Luojus et al., 2010).

63
64 Lastly, there are modeled snow datasets, like the Snow Data Assimilation project with a spatial extent that covers large portions of
65 North America (SNODAS; NOHRSC, 2004). There are physically-based snow models that produce snow information on
66 catchment- to hemisphere-scales, like iSnowBal, SnowModel, Alpine3D, PBSM, and SNOWPACK, among many others (Marks
67 et al., 1999; Liston & Elder, 2006a; Lehning et al, 2006; Pomeroy et al., 1993; Lehning et al., 1999). Studies that integrate all of
68 these types of snow information, *in-situ* observations, RS datasets, and process models, are becoming common in snow research
69 because they often produce the best results (Sturm, 2015).

70
71 Assimilation of data into process modeling is a strategy that seeks to incorporate measurements of environmental variables into
72 the model chain as a 'hybrid' approach to predicting modeled state variables (Carrassi et al., 2018; Kalnay, 2003). There are many
73 examples of data assimilation in the atmospheric sciences and weather prediction (Rabier, 2005), in weather reanalysis products
74 (Gelaro et al., 2017; Kalnay et al., 1996; Messinger et al., 2006; Saha et al., 2010), in the hydrological sciences (Han et al., 2012;
75 McLaughlin, 2002; McMillan et al., 2013; Park and Xu, 2013), and also in snow science (SNODAS; NOHRSC, 2004; Carroll et
76 al., 2001). Data assimilation schemes in snow science rest on the notion that modeled variables like SWE can be merged with an
77 *in-situ* observed value at the same location and time using an objective function. This objective, or cost, function quantifies the
78 differences between the modeled state variable and the observed state (Reichle et al., 2002; Reichle, 2008; McLaughlin, 2002).
79 These methods can assimilate model state variables, like SWE, using a statistical method like a Kalman filter or they can assimilate

80 model fluxes like snowfall precipitation or snowmelt rates (Carroll et al., 2001; Clark et al., 2006; Magnussen et al., 2014; Reichle,
81 2008). Other direct insertion assimilation schemes in snow science run the model twice, once without the assimilated data, and a
82 second time after the *in-situ* observations and correction factors are calculated in order to produce an updated state variable (Liston
83 and Hiemstra, 2008; Malik et al., 2012; Helmert et al., 2018). Regardless of the method of assimilation, the goal is the same: to
84 produce a more accurate modeled state variable (snow depth or SWE) in space and time and to reduce uncertainty in the state
85 variable by using *in-situ* observations to modify the process model output.

86
87 Snow depth measurements are a type of *in-situ* snowpack observation that can be made accurately and quickly by anyone with a
88 measuring device. The potential of mobilizing a new type of in-situ snow dataset collected by snow professionals and snow
89 recreationists is significant because these participants often travel to remote mountainous environments worldwide where in-situ
90 snow observations are sparse. Consequently, the current study turns to citizen scientists for snow data collection. Citizen science
91 is a unique tool for research in which scientists request input from the general public on data collection, data analysis, or data
92 processing (McKinley et al., 2017; Silvertown, 2009; Wiggins and Crowston, 2011). Through citizen science efforts, researchers
93 access data that are either highly decentralized or concentrated in space, as well as obtain measurements frequently or randomly
94 in time. The primary advantage is that many people can accomplish data collection at spatial and temporal scales well beyond the
95 capacity of a single researcher or small group of scientists (Bonney et al., 2009; Cooper et al., 2007; Dickinson et al., 2010). Recent
96 successful citizen science-based research includes the CrowdHydrology project that monitors stage heights of streams and rivers
97 (Fienen and Lowry, 2012; Lowry and Fienen, 2013), and the CrowdWater project, which obtains multiple types of crowdsourced
98 measurements of hydrological variables using a publicly available app (Seibert et al., 2019; van Meerveld et al., 2017). Buytaert
99 et al. (2014) provides a comprehensive review of the recent challenges and motivations of citizen science in hydrology. This unique
100 type of data collected by citizen scientists has been used in many natural sciences, and snow hydrology represents a new opportunity
101 for citizen science-based research.

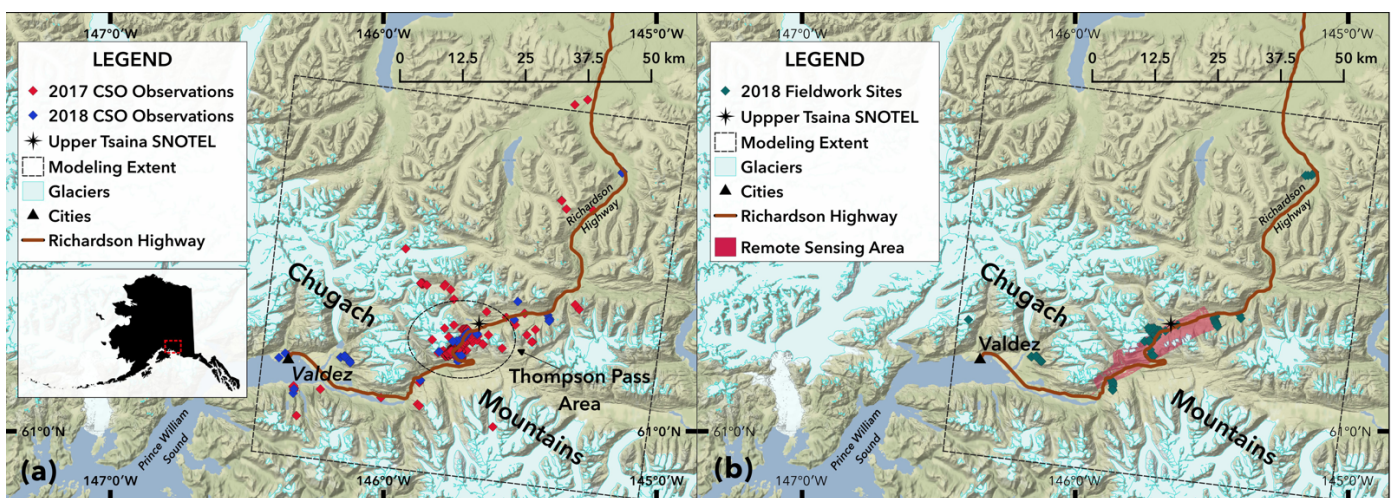
102
103 The present study explores the assimilation of a unique type of citizen science-based data in snow modeling: snow depth
104 measurements collected by citizen scientists traveling in snow covered landscapes worldwide. This new snow dataset and project
105 is called Community Snow Observations (CSO; communitysnowobs.org). The CSO campaign relies on backcountry recreationists
106 including skiers, snowboarders, snowmachiners, cross country skiers, snowshoers, and snow professionals, including avalanche
107 forecasters and snow scientists, who visit snowy environments for work and recreation to obtain snow depth measurements of the
108 snowpack (Hill et al., 2018; Yeeles, 2018). Other citizen science projects are underway in snow science, including research on the
109 relationship between vernal windows and snow depth (Contosta et al., 2017), snow depth observations using Twitter (King et al.,
110 2009), and the backyard precipitation measurement campaign called Community Collaborative Rain, Hail, and Snow Network
111 (Reges et al., 2016). The CSO project adds to a growing body of research accomplished by citizen scientists in the natural sciences,
112 and demonstrates how CSO measurements can be assimilated into the process model workflow using a simple data assimilation
113 technique to sometimes improve model results..

114
115 The current study aims to answer two questions. First, can citizen scientists' snow depth measurements be incorporated into the
116 process model workflow in a way that improves model performance? This question is addressed by presenting an ensemble of
117 modeled snow depth and SWE distribution results with two types of outputs: (a) a set of model outputs without any snow depth
118 measurements assimilated and, (b) a set of model outputs with CSO snow depth measurements assimilated. To answer this first

119 question, we characterize the results using temporal and spatial datasets for validation. These datasets include time-series SWE
120 observations at a SNOTEL station in the study area and LiDAR- and photogrammetry-derived snow depth maps from 2017 and
121 2018. We rely upon common metrics for characterizing the spatial distribution of modeled versus observed continuous
122 environmental variables to assess the value of the CSO modified outputs (Riemann et al., 2010). Secondly, how do the results vary
123 with the number of the CSO measurements assimilated? We address this question by randomly selecting and varying the quantity
124 of CSO measurements in the ensemble members.
125

126 2 Study Area

127 The study focuses on a 5,736 km² area of the eastern Chugach Mountains near Valdez, Alaska, USA (Figure 1a). This high-relief,
128 glacier-carved landscape ranges from sea-level in Port Valdez to rugged peaks exceeding 2200 m.a.s.l., and a mountain pass on
129 the Richardson Highway, named Thompson Pass (815 m.a.s.l.). This region of the Chugach Mountains receives extreme amounts
130 of snowfall, with Thompson Pass holding multiple snowfall records for the state of Alaska, including the 1-day total (1.57 m), 2-
131 day total (3.06 m), and weekly total (4.75 m; Shulski and Wendler, 2007). Like other places in the Chugach Mountains, snow
132 densities and snow depths in the region vary greatly across short distances (Wagner, 2012). There are deep, dense, and wet
133 snowpacks found in the maritime coastal zone. The interior regions of the Chugach Mountains further from the coast contain
134 shallower, less-dense, and drier snow climates (Sturm et al., 1995; Sturm et al., 2010a). These factors are important because the
135 Thompson Pass region and the Chugach mountains are frequently accessed by backcountry skiers and snowboarders, backcountry
136 snowmachiners, and multiple heli-skiing operations due to the exceptional access to steep terrain, and deep, mountain snowpack
137 (Carter et al., 2006; Hendrikx et al., 2016). Due to the popularity of the area for backcountry snowsports and the risk of danger for
138 avalanches affecting highway conditions, the Valdez Avalanche Center produces avalanche forecasts for many of the slopes
139 adjacent to the Richardson Highway in the Thompson Pass region. The choice of a study area within a mountainous region visited
140 regularly by snow recreationists and professionals is essential for the present study. For these reasons, the Thompson Pass region
141 of the Chugach Mountains in Alaska was selected for the initial phases of the CSO project.
142



143
144 **Figure 1: Study Area Map and Fieldwork Sites.**
145 **(a) The study area maps showing the Community Snow Observations (CSO) measurements, the modeling spatial extent, and the**
146 **Thompson Pass region of the Chugach Mountains. (b) The 2018 fieldwork includes 72 sites with co-located snow water equivalent and**

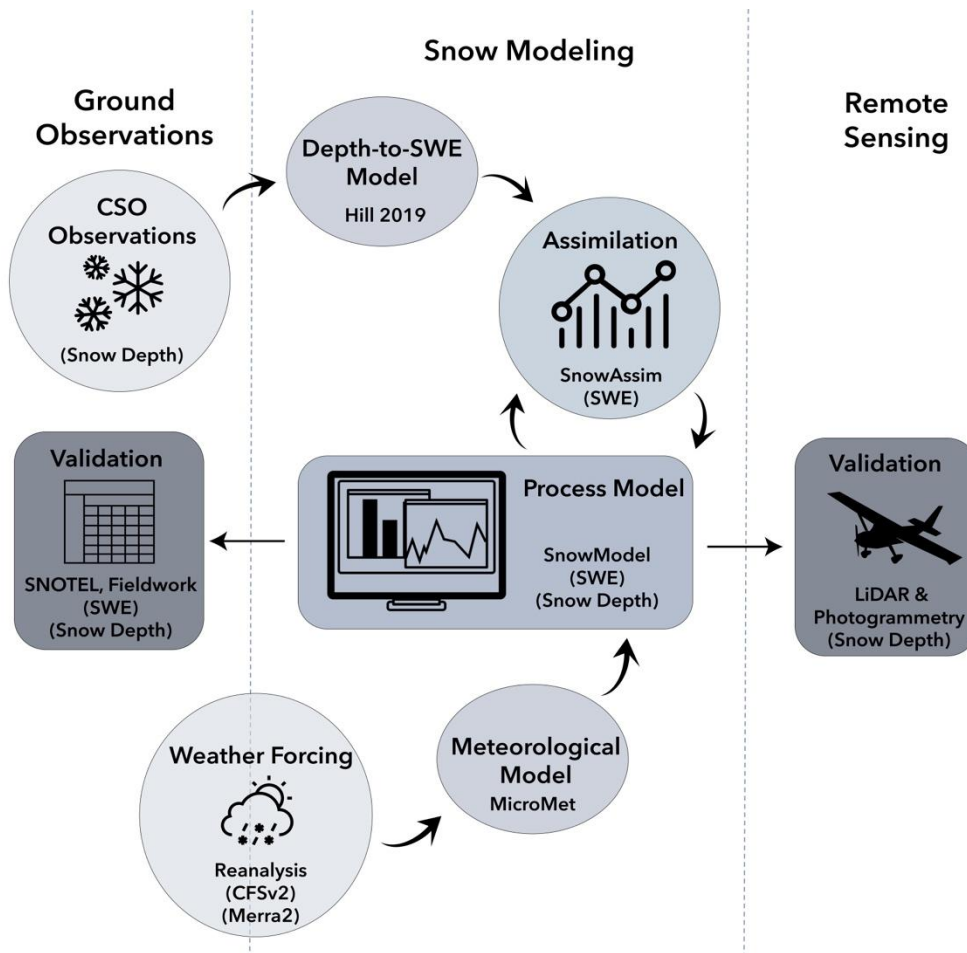
147 snow depth measurements. The remote sensing datasets from 2017 and 2018 are overlain on the map, along with the location of the
148 Upper Tsaina SNOTEL station.

149 3 Methods and Datasets

150 3.1 Model Dataflow

151 This study relies on a common research design in snow science that uses (1) *in-situ* snow observations, (2) physically-based process
152 modeling, and (3) remote sensing of the snowpack to accomplish its primary objectives (Sturm, 2015). Figure 2 is a conceptual
153 diagram of how the citizen scientists' snow depth measurements fit into the model chain for the present study. The modeling
154 process begins with the weather forcing products and citizen scientists' snow depth observations as model inputs. Sub-models for
155 meteorological variable distribution, snow depth to SWE estimation, and for the assimilation of snow measurements are employed
156 before the final simulation occurs. The process model outputs are then validated by the RS datasets, the SNOTEL station record,
157 and the 2018 field measurements. Incorporating the citizen scientists' observations into the model chain is an attempt to modify
158 the model outputs by *in-situ* snow depth observations.

159



160

161

162

163

164

165

Figure 2: Model Dataflow Diagram.

The model chain begins with the weather forcing product and the Community Snow Observations (CSO) datasets. The arrows indicate dataflow through the series of sub-models to the process model output. The model output is then validated by the SNOTEL station time-series, the 2018 fieldwork, and the remote sensing datasets.

166 **3.2 Modeling Framework**

167 In this study we used a sequence of models to simulate SWE and snow depth distributions within the Thompson Pass study area
168 during WY2017 and WY2018. The sections below provide brief information about the models used in this study. For more details,
169 please refer to the source citations for each model.

170

171 **3.2.1 SnowModel**

172 SnowModel (Liston & Elder, 2006a) is a physically-based, spatially distributed process model for simulating the evolution of
173 snowpacks in snowy environments, and has been used for high-resolution and hemispheric-scale modeling worldwide (Beamer et
174 al., 2016; Beamer et al., 2017; Crumley et al., 2019; Liston and Hiemstra, 2011; Mernild et al., 2017a-b). We chose SnowModel
175 for the Chugach Mountains study area because it contains a data assimilation sub-model, SnowAssim, and a snow transportation
176 sub-model, SnowTran3d. Within SnowModel, various other sub-models solve the energy budget for the snowpack, generate runoff
177 quantities, etc. The present study focuses on the snow depth and SWE distribution outputs from SnowModel from simulations with
178 and without the data assimilation sub-model.

179

180 **3.2.2 MicroMet**

181 MicroMet (Liston & Elder, 2006b) is a meteorological distribution sub-model for weather station or reanalysis datasets that can be
182 paired with SnowModel in spatially explicit modeling applications. MicroMet uses the Barnes objective analysis scheme for
183 interpolating meteorological input variables to the gridded SnowModel domain for each model timestep (Barnes, 1964; Barnes,
184 1973). In the present study, instead of using local weather station data, the model is forced with reanalysis data and MicroMet uses
185 the node locations as weather stations, accessing the reanalysis node surface level precipitation, wind speed and wind direction,
186 relative humidity, air temperature, and elevation variables for the spatial interpolation. MicroMet has been paired with reanalysis
187 weather products and SnowModel in many studies worldwide (Baba et al., 2018; Beamer et al., 2016; Liston & Hiemstra, 2011;
188 Mernild et al., 2017a).

189

190 **3.2.3 SnowTran3d**

191 Wind redistribution of snow is an important factor for the spatial distribution of snow depths and SWE distributions for snow
192 modeling (Clark et al., 2011). Wind events build snow deposits in the gullies and the leeward side of bedrock features into drift
193 depths greater than 10 m at times within the Thompson Pass study area. These events also leave some portions of the landscape
194 completely scoured and void of snow based on fieldwork observations and the RS snow surveys from both years. SnowTran3d is
195 a sub-model within SnowModel that redistributes the snow laterally in the model grid according to the processes that govern snow
196 transportation: fetch, wind speed, wind direction, wind shear stress and the shear strength of the snowpack, saltation and turbulent
197 suspension of the snow, and sublimation (Liston et al., 2007). SnowTran3d is suitable for use as a sub-routine within SnowModel
198 when the model grid cell resolution is appropriate for the length scale of snow transportation processes to occur, for example,
199 primarily at model resolutions less than 100 m.

200

201 **3.2.4 SnowAssim**

202 To assimilate the CSO measurements, we used the sub-model SnowAssim developed in tandem with SnowModel (Liston and
203 Hiemstra, 2008). The SnowAssim data assimilation scheme is relatively simple when compared to other assimilation methods.
204 Direct insertion methods often insert the observed state values into the modeled field in the locations and times where data is
205 available (McGuire et al., 2006; Fletcher et al., 2012). Hedrick et al. (2018) outlines a ‘modified’ direct insertion method, where
206 Airborne Snow Observatory LiDAR-based snow depth distributions are input into the iSnobal workflow to modify model state
207 variables before a new initialization of the model begins. Liston and Hiemstra (2008) describe a different type of modified direct
208 insertion assimilation scheme (SnowAssim) used in the present study. SnowAssim requires the model to be run twice and pauses
209 at the end of the first model run. During this pause, differences between the observed SWE depths and modeled SWE depths in
210 time and location are calculated and interpolated to the entire model domain in the form of a correction surface. The final correction
211 surface is spatially distributed (for each day of observations) using the Barnes interpolation scheme. These correction surfaces are
212 then applied to the precipitation inputs and snowmelt factors during the second model run.

213

214 Note that CSO measurements are submitted as snow depth (m), but the SnowAssim model code and physical equations require
215 observational inputs to be SWE depth (m), so a conversion from depth to SWE was necessary. The snow depth to SWE conversion
216 method for the current study will be discussed in the following section. The model determines the dominant snow season phase
217 (accumulation or ablation) and applies the correction factor surface to either a) the precipitation fluxes or b) the snowmelt factors
218 during the second model simulation. Additionally, the Barnes interpolation scheme determines outliers within the observed dataset
219 and determines the degree to which the assimilated values fit the modeled values. This determination creates a smoothed
220 representation of the observed dataset in the assimilation results. For extensive details about the data assimilation scheme, see
221 Liston and Hiemstra (2008), their section 3, 4, and 5.

222

223 Other data assimilation methods include particle-batch smoother and particle filters. These are Bayesian data assimilation methods
224 used to estimate system state variables based on predicted estimates (modeled) and noisy measurement data (observed). These
225 types of data assimilation methods rely heavily on characterizing and incorporating the predicted estimate uncertainties and
226 measurement uncertainties into the analysis using probability distribution functions (Magnusson et al. 2017; Margulis et al. 2015).
227 In direct insertion or modified direct insertion methods like SnowAssim, modeled and observed state variable uncertainties are not
228 explicitly characterized.

229

230 **3.2.5 Snow Depth to Snow Water Equivalent Conversion**

231 CSO participants take measurements of snow depth yet SnowAssim requires SWE observation inputs. A conversion from snow
232 depth to SWE was necessary for the present study. A body of research exists on the best methods for converting point measurements
233 from snow depth to SWE, using either bulk density estimations, snow climate classifications, statistical models, or atmospheric
234 conditions and energy balance approaches (Sturm et al., 1995; Sturm et al., 2010a; McCreight et al., 2014; Jonas et al., 2009;
235 Pagano et al., 2009; Hill et al., 2019; Pistocchi, 2016). The Hill et al. (2019) model was chosen for two reasons. First, the data
236 requirements are minimal for this model, requiring only location, day of water year (DOY) and readily-available climatological
237 information based on input location. These minimal requirements align with the information available from CSO measurements.

238 Second, it was found to outperform other bulk density methods such as Sturm et al. (2010) and Jonas et al. (2009) when tested
239 against a wide variety of snow pillow and snow course datasets, with an overall bias of 0.2 cm and RMSE in SWE of 6 cm (Hill
240 et al., 2019).

241

242 **3.3 Model Input Datasets**

243 **3.3.1 Elevation and Land Cover**

244 SnowModel requires a digital elevation model (DEM) and a land cover model as two of the three primary input datasets. The DEM
245 is the National Elevation Dataset (NED) from the United States Geological Survey downloaded at 30 m resolution and then rescaled
246 to 100 m spatial resolution (Gesch et al., 2009). The land cover model is the National Land Cover Database (NLCD) 2011 dataset
247 at 30 m spatial resolution and then resampled to 100 m resolution (Homer et al., 2015). The NLCD dataset was reclassified to
248 match the land cover input classes required by SnowModel. Initially, we tested results from model simulations at two spatial
249 resolutions, 30 m and 100 m, covering the Thompson Pass model domain. After calibrating the model, the results section only
250 includes the 30m resolution.

251

252 **3.3.2 Weather Forcing Datasets**

253 Various weather reanalysis products have been used in remote portions of Alaska in previous studies (Beamer et al., 2016; Beamer
254 et al., 2017; Crumley et al., 2019; Liston and Hiemstra, 2011). In Alaska, each reanalysis product shows bias corresponding to
255 meteorological variable, regional location, and season of the year (Lader et al., 2016; see their Figures 3 and 4). For this reason,
256 the current study considered two weather reanalysis products that differ in their biases in temperature and precipitation in the
257 Thompson Pass region during the winter and the summer seasons. We used the Climate Forecast System Reanalysis version 2
258 product (CFSv2) and the Modern-Era Retrospective Analysis for Research and Applications version 2 (MERRA2) product for the
259 weather forcing inputs for SnowModel. The CFSv2 product from the National Centers for Environmental Prediction is an extension
260 of the lower spatial resolution Climate Forecast System Reanalysis (CFSR) version 1 product that began in 1979 and the version
261 2 product became available in 2011 (Saha et al., 2010). The CFSv2 data are available at a spatial resolution of 0.2 arc degrees, and
262 a 6 hour temporal resolution (Saha et al., 2014). The CFSv2 dataset was downloaded using Google Earth Engine (GEE), a platform
263 for accessing and analyzing scientific datasets with global coverage. The MERRA2 weather reanalysis product from NASA's
264 Global Modeling and Assimilation office is the second meteorological forcing dataset tested in the present study (Gelaro et al.,
265 2017). The MERRA2 data are available at a spatial resolution of 0.667 degrees by 0.5 degrees, with a 3 hour temporal resolution
266 beginning in 1979. MERRA2 replaces the older version product with updated assimilation processes to include more weather
267 datasets.

268

269 **3.4 Snow Datasets**

270 **3.4.1 Snow Telemetry Station Data**

271 The study area contains two SNOTEL stations operated by NRCS. The first station is the Upper Tsaina SNOTEL (UTS) station
272 located at 534 m.a.s.l. on the NE side of Thompson Pass reporting the full standard set of sensor variables, including precipitation,

273 temperature, snow depth, and SWE. The second station is the Sugarloaf Mountain SNOTEL (SLS) station, located near the Valdez
274 Arm of the Prince William Sound at 168 m a.s.l. in the SW corner of the study area and records only precipitation, temperature,
275 and snow depth, but not SWE (Figure 1). The SLS station data was used to create local temperature lapse rates for the calibration
276 and the UTS station data was used in the manuscript results section to create the SWE time series analysis. Detailed information
277 about the SNOTEL sensors and climate monitoring instruments can be found at the SNOTEL website
278 (<https://www.wcc.nrcs.usda.gov/snow/>) and Serreze et al. (1999). Direct links to the SNOTEL websites for the UTS and SLS
279 stations can also be found in Section 10 below.

280

281 **3.4.2 LiDAR and Photogrammetry Derived Data**

282 An aerial photogrammetric survey was conducted on April 29, 2017 with a Nikon D800 36.2 megapixel camera flown on a fixed-
283 wing aircraft above a portion of the Thompson Pass study area, see Figure 1b for location and extent. An onboard Trimble Global
284 Navigation Satellite System (GNSS) and a base-station were used for positional control. Post-processing was completed with
285 structure-from-motion software to create a digital surface model (DSM) of the photogrammetry-derived snow surface. An airborne
286 LiDAR survey was collected on April 7th and 8th, 2018, using a Riegl VUX1-LR laser scanner flown on a fixed-wing aircraft. An
287 onboard integrated inertial measurement unit (IMU) and GNSS, and a base-station were used to provide positional control for the
288 LiDAR-derived snow DSM. Both RS datasets were evaluated against a previously collected photogrammetry-derived DSM from
289 2014 when no snow was present. An interpolation scheme was used to gap-fill some of the negative values in the snow DSM due
290 to vegetation cover effects. There is uncertainty associated with the RS dataset acquisitions, and the sources of error are related to
291 flight trajectory and geometry, laser scan angle, density of vegetation and canopy, and steep gradients in the terrain (Deems and
292 Painter, 2006). The vertical RMSE in snow depth for the photogrammetry and LiDAR datasets are estimated at 31.0 cm and 10.2
293 cm, respectively. While we acknowledge and report these error estimations, they are integrated into the results in Table 3 in Section
294 6.5 but not used in the spatial results reported in Section 6.2.

295

296 **3.4.3 Chugach 2018 Fieldwork Data**

297 Three weeks of fieldwork in the Thompson Pass region were conducted in March, April, and May of 2018. Snow depth and SWE
298 were measured throughout the study area with an avalanche probe and a Federal Snow Sampler. At each fieldwork measuring site,
299 a central SWE measurement was taken using the Federal Sampler. Avalanche probes were used in the surrounding 100 m² to take
300 a series of 8 snow depth measurements extending 5 m in each direction from the central SWE measurement. Federal sampler data
301 collection introduces uncertainty in the form of measurement error due to variable snow conditions and densities, hard impenetrable
302 crusts, and loss during extraction. Dixon and Boon (2012) report the results of several studies showing that the Federal Sampler
303 error, as a percentage of SWE depth, ranges from 4.6% to 11.2%. Our results presented in Section 6.5 include field measurements
304 of SWE that use the higher 11.2% value for conservative SWE error estimation.

305

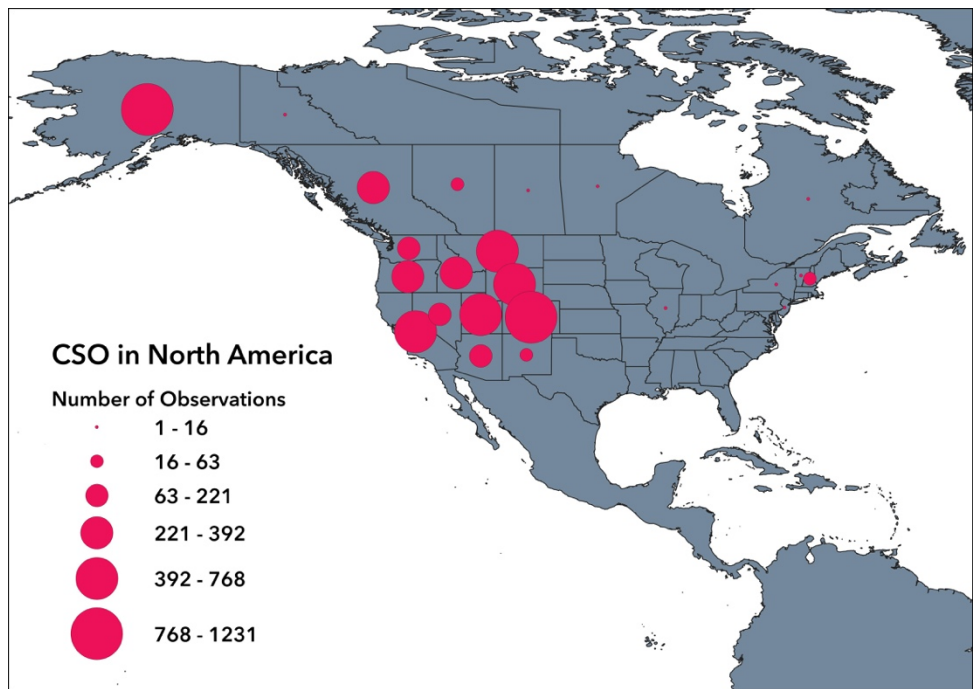
306 The fieldwork sampling protocol was designed to consider: (1) variability in snow depth in small areas less than 100 m², (2) month-
307 to-month changes in snow depth and SWE, and (3) spatial gradients in snow density throughout the entire study area. A diagram
308 of the location of each observational site can be found in Figure 1b. The 2018 fieldwork dataset was used for validation with two

309 purposes in mind. First, the 2018 fieldwork SWE measurements were used as a validation dataset for the 2018 SWE distribution
310 results. Secondly, since the data collected in the spring of 2018 contains measured snow depths and SWE at 70 observational sites
311 (n = 560; 8 per site), we conducted an analysis of the sub-grid scale variability in snow depth found at each observational site and
312 these results are found in the discussion section.
313

314 3.4.4 Community Snow Observations Data

315 The CSO program collects snow depth data from citizen scientists in snowy environments worldwide. Full details including links
316 to smartphone apps and tutorials are found at <http://communitysnowobs.org>. Citizen scientists take several (2 to 4) snow depth
317 measurements within a small area (< 4 m²) using an avalanche probe or other depth measuring device (meterstick, etc.). These
318 measurements are then averaged by the participant and submitted using the app or program preferred by the participant. The
319 submitted data include the global positioning system (GPS) location in latitude and longitude, time and date, and snow depth
320 measurement (cm). The accuracy of the GPS system for each participants' mobile device determines the location error of the GPS,
321 with common errors for mobile phones ranging between ±4 to 7 m (Garnett and Stewart, 2015; Schaefer & Woodyer, 2015). Since
322 the model resolution is 30 m and 100 m, this level of horizontal error in GPS location is acceptable for the purposes of our research
323 questions. All collected data are made freely available on the CSO website for visualization and download (see Section 9 for Data
324 Availability). Thousands of measurements have been recorded by participants in CSO globally since it began in January 2017 with
325 initial measurement campaigns in Alaska and other frequently visited locations in mountain regions across North America (Figure
326 3). In the modeling domain of the current study, 442 CSO measurements were available for WY2017 and 104 CSO measurements
327 for WY2018. These measurements were concentrated in the Thompson Pass region of the study area (Figure 1) and range from 25
328 m to 1400 m in elevation.
329

329



330

331 **Figure 3: CSO Participation in North America.**
 332 **Participation in the Community Snow Observations (CSO) project in North America aggregated by the number of observations**
 333 **recorded in each U.S. state or Canadian province between January 1st, 2017 and December 31st, 2019.**

334
 335 **4 Calibration**

336 We performed model calibration using five years of the historical record of the UTS station from WY2012 through the end of
 337 WY2016. The calibration was focused on adjustments to temperature lapse rates, precipitation lapse rates, wind adjustment factors,
 338 and use of the SnowTran3d sub-model. We chose temperature lapse rates and precipitation lapse rates for calibration because
 339 SnowModel is known to be limited by these factors when large elevational differences exist within the model domain (Liston and
 340 Elder, 2006a). We chose wind adjustment factors and the wind transportation sub-model for calibration because wind redistribution
 341 of snow plays a significant role in the study area based on the 2018 fieldwork and the RS surveys from 2017 and 2018. Since the
 342 SnowAssim sub-model requires a single layer snowpack, no adjustments were made to the snowpack layer structure. For each
 343 weather reanalysis product, a full calibration was performed for the 30m and 100m model resolutions, in the event that spatial
 344 resolution plays a significant role in parameter selection. See Appendix A for the descriptions of the model parameters tested
 345 during the calibration.

346
 347 The daily SWE output from each calibration simulation is compared with the UTS observed SWE for the duration of the 5-year
 348 calibration time period using root mean squared error (RMSE), the Nash Sutcliffe Efficiency (NSE), the Kling-Gupta Efficiency
 349 (KGE), and mean bias error (Bias) to assess the calibration simulations. Table 1 lists the best 30m and 100m calibration simulations,
 350 based on their time-series RMSE, NSE, KGE, and Bias scores. We acknowledge that measurement errors can occur with SNOTEL
 351 snow pillows and that these well-known errors may affect the accuracy of the observational dataset (Johnson and Schaeffer, 2002;
 352 Johnson, 2003).

353
 354 **Table 1: Model Calibration Results.**
 355 **The best calibration results are given for each set of simulations for water years 2012-2016, along with the root mean squared error**
 356 **(RMSE), the Nash Sutcliffe Efficiency (NSE), the Kling-Gupta Efficiency (KGE), and the mean bias error (Bias).**

Reanalysis Product & Resolution	Time Step	Number of Simulations	RMSE SWE (cm)	NSE	KGE	Bias SWE (+/- cm)
MERRA2, 30m	3hrly	45	24	-0.29	0.08	+16
MERRA2, 100m	3hrly	45	26	-0.10	-0.10	+19
CFSv2, 30m	6hrly	45	22	-0.15	-0.01	+17
CFSv2, 100m	6hrly	45	22	-0.15	-0.01	+17

357
 358 Calibration results in Table 1 show that the 30m model grid resolution slightly outperforms the 100m model grid resolution in the
 359 MERRA2-forced calibration simulations. However, the CFSv2-forced simulations show no difference between the model grid
 360 resolutions. The CFSv2 product slightly outperforms the MERRA2 product in terms of SWE RMSE. Overall, the differences
 361 between the top performing model grid resolution and reanalysis product are mixed and potentially negligible, varying by metric.
 362 The NSE and KGE model performance metrics in the calibration simulations are lower than expected, due primarily to precipitation

363 inputs from the reanalysis products that were consistently higher than measured precipitation at the UTS station (see the following
364 paragraph for more details). The SnowModel default parameter values notably and consistently produce the top performing
365 simulations, see Appendix B for details. Due to each of these factors, the calibrated model for the remainder of the study uses the
366 CFSv2 reanalysis product, the 30m model grid resolution, and the SnowModel default parameter values.

367
368 One of the primary obstacles for process modeling is the availability of accurate weather input data, and the related uncertainties
369 with weather inputs are a well-known complication in snow and hydrological modelling (Rivington et al., 2006; Schmucki et al.,
370 2014; Schlögl et al., 2016). Initial tests of modeled precipitation fields using Micromet versus the observed precipitation at the
371 UTS station revealed that both reanalysis products overestimated the amount of precipitation observed in the study area at the UTS
372 station, see Appendix C. The CFSv2 precipitation totals at the UTS station were nearly 1.6 times the measured precipitation at the
373 UTS station during the calibration period. The improvements that could be gained by adjusting a subset of the model parameters
374 (wind, temperature, and precipitation lapse rates due to differences in elevation and season) during calibration were not likely to
375 overcome this extreme precipitation deficiency, explaining why the final calibrated NSE and KGE values were low. There are two
376 ways to address this precipitation deficiency using SnowAssim. One is to adjust the precipitation inputs during calibration, and the
377 other is to allow the assimilation to adjust the precipitation inputs. Both ways are functionally equivalent because they apply a
378 simple, scalar-based correction surface to the precipitation fluxes. In our calibration process we chose to use SnowAssim to address
379 the precipitation deficiencies in the reanalysis product, following the approach of other recent studies in mountainous regions of
380 Alaska, and following the original purpose of the SnowAssim model (Cosgrove et al., 2021, their Calibration of SnowModel
381 section; Liston and Heimstra, 2008; Young et al., 2020, their section 3.4). This calibration decision supports the primary goal of
382 the current study, which is to test whether or not participant-submitted snow depth measurements can improve physically-based
383 modeling efforts through data assimilation.

384
385 These calibration results and the precipitation deficiencies motivated us to design an experiment to supplement the main findings
386 of this research. For this experiment we introduced a model precipitation adjustment factor similar to the method outlined in
387 Mernild et al. (2006). We applied this scalar value to the precipitation fields as a bias correction of the precipitation inputs. We
388 tested 11 precipitation adjustment factors ranging from 0.95 to 0.45 and applied them to the meteorological forcing inputs during
389 the 5-year calibration time period. For more details about the precipitation and precipitation adjustment factor results, see Appendix
390 D. This experiment, with summary results presented in section 6.6, allows us test improvements in model performance when the
391 precipitation inputs are bias corrected prior to model assimilation of CSO measurements.

392
393

394 **5 Experimental Design**

395 We carried out a series of simulations in order to (1) quantify the improvement in model performance due to the assimilation of
396 CSO measurements and to (2) understand the effects of the number of CSO data points selected for assimilation. First, we set up
397 geographic and temporal requirements for the assimilated data. The only geographic requirement was that the CSO measurements
398 must be located within the larger 5,736 km² model domain. We subset the CSO measurements temporally to the peak SWE time
399 period or later. According to the UTS station, peak SWE in the study area generally occurs mid- to late-April and consequently the

400 earliest assimilation date was set to April 15th. The CSO measurements were aggregated by week by assuming all measurements
401 in a given week occurred on the same day for the purposes of assimilation. This weekly aggregation allows the correction surfaces
402 generated by SnowAssim time to adjust the precipitation fluxes and snowmelt factors between observations, thereby altering the
403 model outputs during assimilation. Additionally, CSO participation in the Thompson Pass region during the early accumulation
404 season was infrequent in WY2018 and non-existent in WY2017. Since peak SWE is important for mountain hydrology and
405 ecology, with many snow studies using it as an indicator metric, the time restrictions are acceptable for the research questions
406 addressed in this study (Bohr and Aguado, 2001; Trujillo et al., 2012; Kapnick and Hall, 2012; Mote et al., 2018; Wrzesien et al.,
407 2017).

408

409 With these geographic and temporal filters defined for assimilation, we decided to vary the number of CSO data points selected
410 for assimilation. Model simulations without CSO measurements provide a baseline for comparison, referred to as the NoAssim
411 case. Ensemble model simulations were carried out with various numbers of CSO measurements assimilated, referred to as the
412 CSO simulation case. An ensemble of 60 trials per year were carried out with $n = 1$, $n = 2$, $n = 4$, $n = 8$, $n = 16$, and $n = 32$, where
413 n equals the number of CSO measurements assimilated per WY. In each instance (n value), 10 realizations of the numerical
414 experiment were carried out. With the ensemble model simulations defined in terms of the spatial and temporal restrictions, the
415 number of CSO measurements was the only feature modified during assimilation.

416

417 **6 Results**

418 The following results reflect the three types of available validation datasets: 1) time-series SWE results at the UTS station, 2)
419 spatial snow depth distributions from the RS datasets, and 3) point-based snow depth and SWE measurements from the 2018
420 fieldwork.

421

422 **6.1 Temporal Results Using the Upper Tsaina SNOTEL Station**

423 The temporal results compare the UTS station SWE time-series to the ensemble member SWE time-series during WY2017 and
424 WY2018. Figure 4 displays the temporal cycle of snowpack accumulation and ablation, and the timing of peak SWE. At the UTS
425 station in the study area, the average WY day of peak SWE is 228, or April 15th. Before this day, the snowpack is generally
426 increasing in SWE and afterwards the snowpack generally enters the ablation period with a reduction in SWE. This temporal cycle
427 can be observed in Figure 4 by following the color gradient. The highest performing (Best) CSO simulation (Figure 4b,e) corrects
428 the slope of the snowpack accumulation and ablation phases when contrasted with the NoAssim accumulation and ablation phases
429 and slopes (Figure 4a,d). These time-series results, in terms of model performance metrics and the snowpack temporal cycle,
430 exhibit SnowAssim's ability to incorporate CSO measurements and improve modeled SWE outputs at the UTS station location
431 throughout the entire snow season.

432

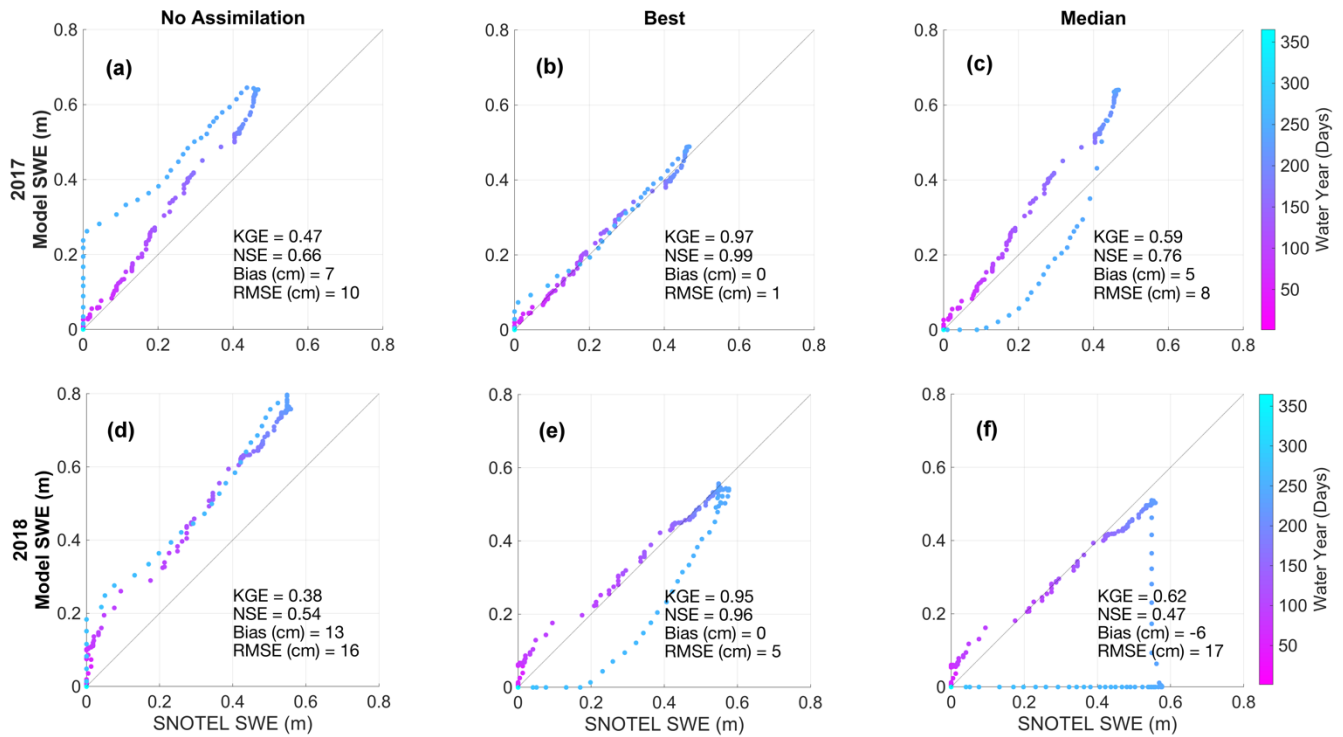


Figure 4: Time Series at Upper Tsaina SNOTEL Station.

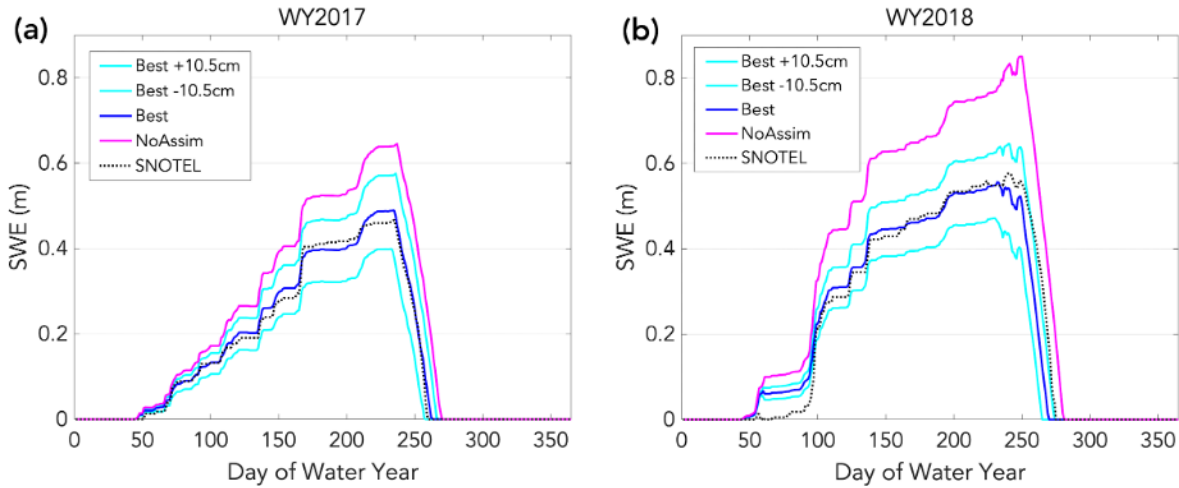
The Upper Tsaina SNOTEL snow water equivalent (SWE) observations versus the modeled SWE for the no assimilation case (a,d), the Best CSO simulation (b,e), and the Median CSO simulation (c,f). The timeseries color gradient corresponds to the day of the water year.

Figure 4 summarizes the temporal results for the Best and median performing (Median) CSO simulations, as well as the NoAssim case. Each ensemble member is evaluated by their KGE, NSE, RMSE, and Bias scores. For results presented in this section, the KGE score is used to rank the ensemble simulations. A full accounting of each ensemble member and their time-series ranking can be found in Appendix E. Modeled SWE depths for the NoAssim case are consistently higher than the UTS station SWE observations for both WYs (Figure 4a,d). The modeled SWE depths for the Best CSO simulation outperform the NoAssim case throughout the entirety of the time-series and represent an improvement in model performance scores according to all of the time-series metrics (Figure 4b,e). The modeled SWE depths for the Median CSO simulation for WY2017 outperform the NoAssim case by all metrics, and the WY2018 Median CSO results are mixed. The ensemble simulation KGE scores outperform the NoAssim KGE scores among 70% of the WY2017 ensemble members, and among 67% of the WY2018 ensemble members. Any number of CSO measurements assimilated show improvements in model performance, a key finding in the time-series results.

Using the snow depth to SWE conversion method during assimilation introduces uncertainty into the modeling process. Instead of using the global estimates of error reported in Hill et al. (2019; RMSE in SWE = 5.9 cm) we decided to calculate this source of error using our fieldwork site measurements. The RMSE in SWE due to the conversion method is 10.5 cm and we perturbed the CSO observations by this amount to depict the upper and lower boundaries of error associated with this source of uncertainty. Figure 5 displays the Best CSO simulation temporal results for each WY, along with the UTS station SWE record and the NoAssim case. These perturbations to the assimilated SWE show improved modeled SWE values at the UTS station when compared to the NoAssim case, even after this source of uncertainty has been accounted for.

457
458
459
460
461
462
463
464
465

Since the timing of snow disappearance is important for ecological systems in alpine environments and water resources managers, we calculated the range in snow disappearance dates from the Best simulations from both water years (see Figure 5 where SWE depth reaches zero between day 250 and 280). In WY2017 and WY2018, the snow disappearance date for the NoAssim case is 10 and 7 days later than the UTS station record, respectively. In WY2017, the snow disappearance date in the Best CSO simulation, accounting for measurement uncertainty, ranges from 3 days earlier to 8 days later than the UTS station. In WY2018, the range is from 10 days to 1 day earlier than the UTS station. These ranges in snow disappearance date are acceptable and show improvements in model performance for some, but not all, of the Best CSO simulations after accounting for measurement uncertainty.

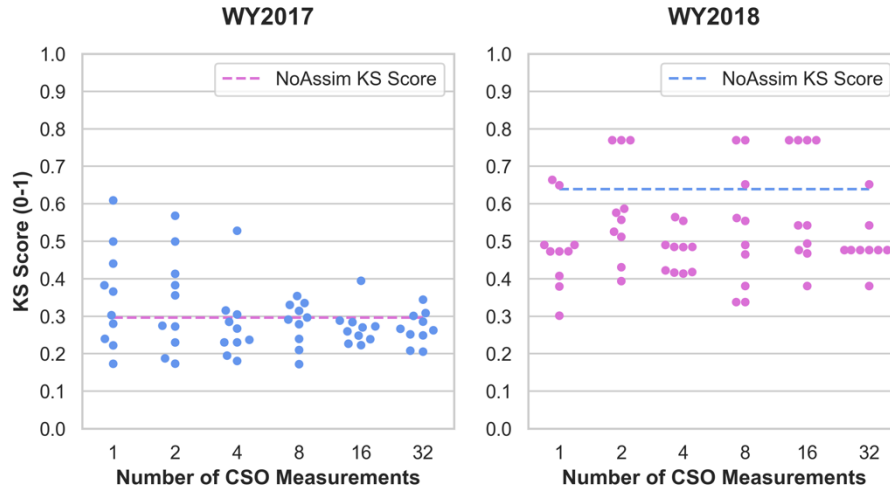


466
467
468
469

Figure 5: Snow water equivalent (SWE) time series results with measurement uncertainty included. The simulations with ± 10.5 cm of SWE represent the upper and lower boundaries of error introduced when converting snow depth measurements to SWE using the Hill et al. (2019) method.

470 6.2 Spatial Results Using the Remote Sensing Datasets

471 The ensemble results are summarized in Figure 6 using the Kolmogorov-Smirnov statistic (KS; Massey, 1951). The KS statistic
472 quantifies the difference between a reference dataset of a continuous variable and a sample dataset of the same variable. The KS
473 statistic represents the maximum distance between the empirical cumulative distribution function (ECDF) of the reference and
474 sample datasets, with KS scores ranging from zero to one, with zero representing perfect dataset agreement (Riemann et al., 2010).
475 In the KS analysis, the reference dataset is the RS derived snow depth distribution and the sample datasets are each of the ensemble
476 snow depth distributions, including the NoAssim case. Figure 6 shows that in WY2017 the CSO simulations are an improvement
477 from the 2017 NoAssim case among 62% of the ensemble members, and in WY2018 among 78% of the ensemble members. Note
478 that only the KS values that fall below the NoAssim line represent an improvement in model performance during the CSO
479 simulations. The spatial results reveal that improvements in model performance are not dependent upon the number of CSO
480 measurements that are assimilated in WY2018. However, WY2017 has a smaller range in KS values as the number of assimilated
481 measurements increases, with more CSO simulations outperforming the NoAssim case. However, WY2017 has a smaller range in
482 KS values as the number of assimilated measurements increases. Additionally, the number of simulations that outperform the
483 NoAssim case in WY2017 gradually increases as the number of CSO measurements increases from 1 to 32. These results also vary
484 according to model performance metric and by WY, with no clear pattern emerging from the number of measurements assimilated.



486
487
488 **Figure 6: Swarmplots of Kolmogorov-Smirnov Scores.**
489 **The ensemble simulations are ranked by Kolmogorov-Smirnov (KS) score per year and plotted according to the number of**
measurements assimilated, including the no assimilation (NoAssim) case.

490

491 The snow depth distribution maps in Figure 7 display the RS datasets (a,b), the results from the Best CSO simulation (c,d), and the
492 NoAssim case for each WY (e,f). Refer to Figure 1 for the RS dataset location within the study area. We present the Best CSO
493 simulation as the focus of Section 6.2 ranked according to KS score ranking (Figure 6). A full accounting of each ensemble member
494 and their spatial distribution ranking can be found in Appendix F. In the RS datasets, there is more variation and heterogeneity in
495 snow depth across short distances (Figure 7a-b). This spatial diversity is evident even after the RS dataset has been aggregated to
496 correspond to the model resolution at 30 m, as depicted in Figure 7. The NoAssim case and Best CSO simulation show less spatial
497 diversity, and the NoAssim case broadly overestimates snow depth when compared to the Best CSO simulation for both WYs. The
498 visualization of the snow depth distributions in Figure 7 illustrates the challenges of accurately representing the process scale
499 through physics-based modeling at low resolutions (Blöschl, 1999), and some of these challenges will be examined further in the
500 discussion section.

501

502

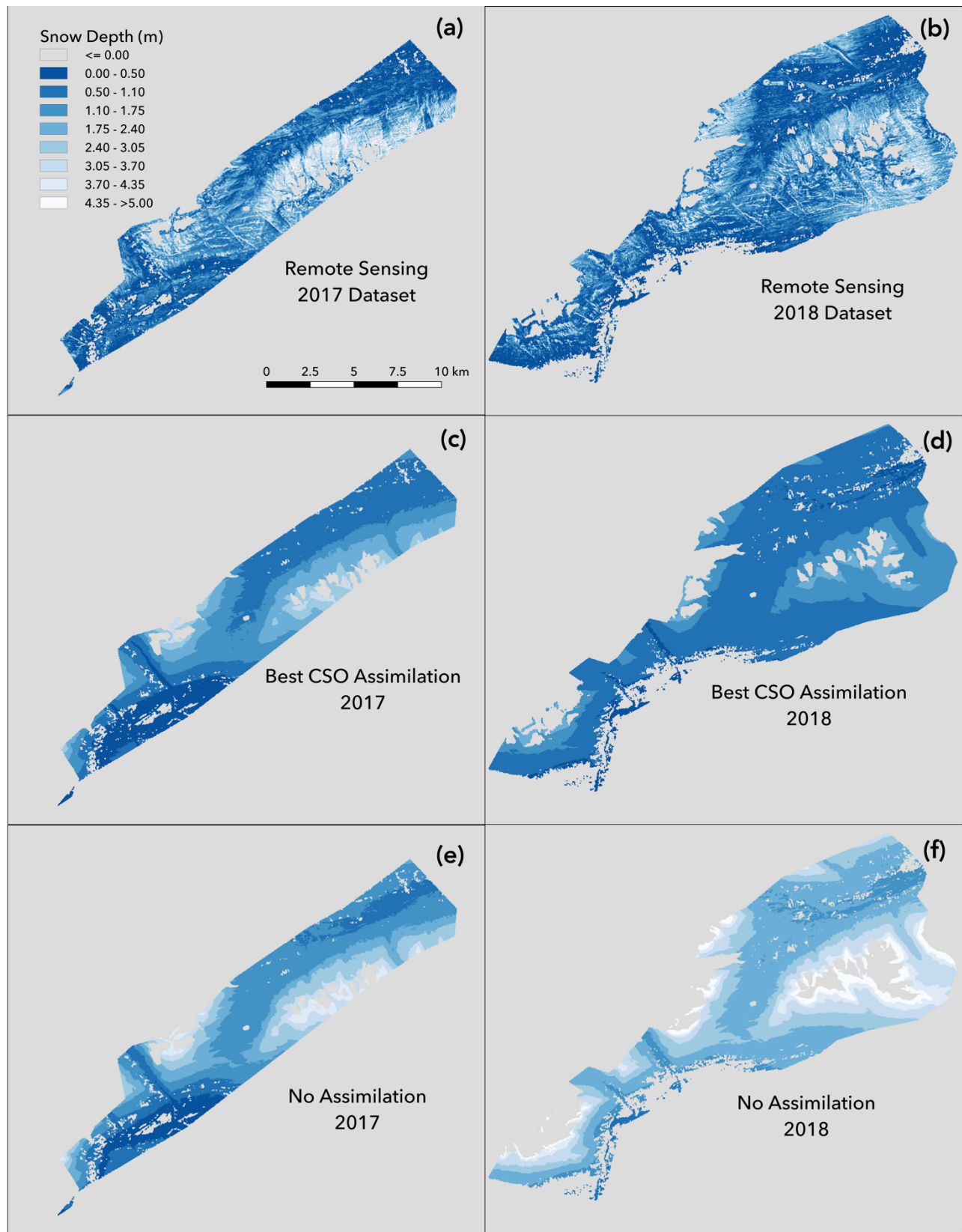


Figure 7: Snow Depth Distribution Maps.

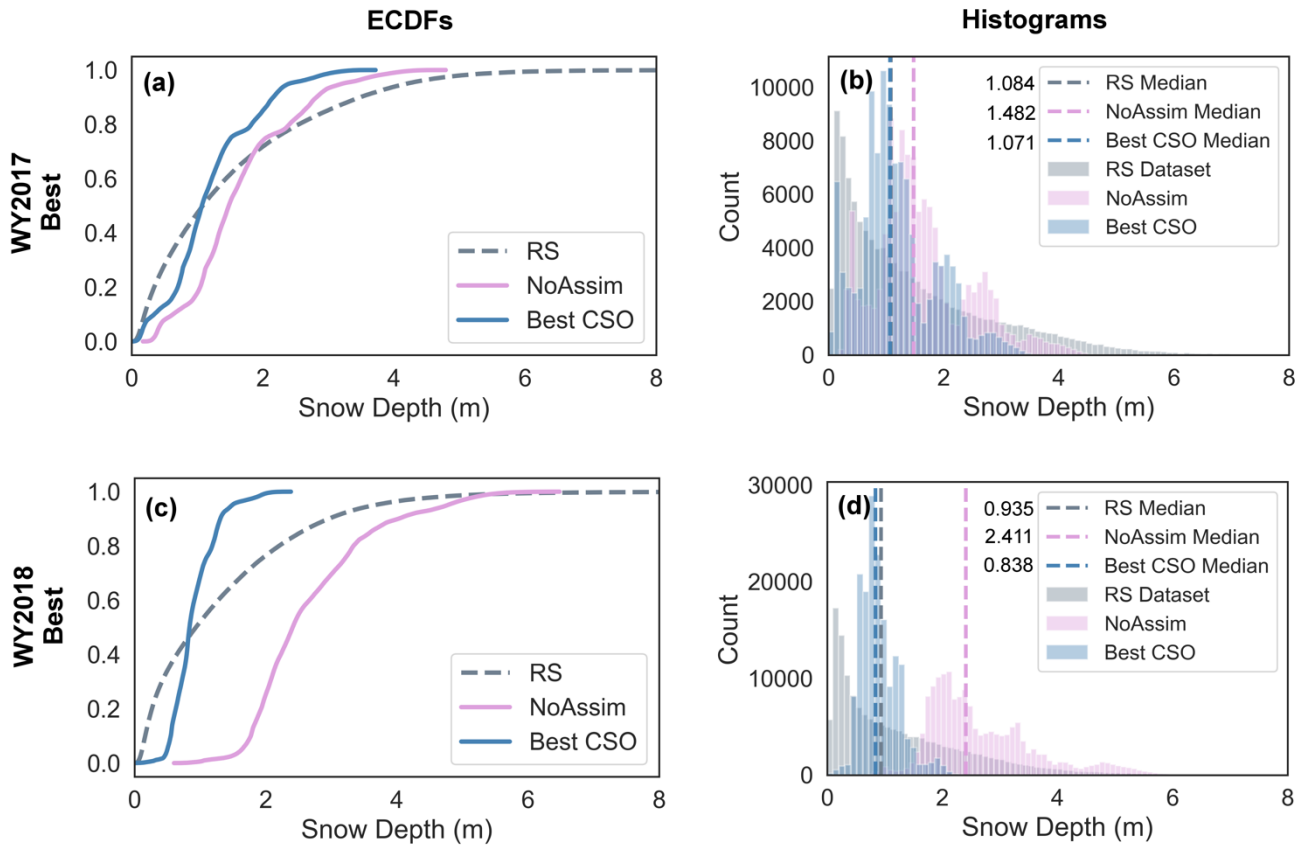
(a,b) The remote sensing (RS) datasets from 2017 and 2018. (c,d) The best CSO simulation results corresponding to the RS dataset spatial extent. (e,f) The no assimilation results corresponding to the RS dataset spatial extent. The total model area that corresponds to the RS dataset in 2017 is 104 km² and 149 km² in 2018.

503
504
505
506
507

508

509 Figure 8 presents histograms and empirical cumulative distribution functions (ECDFs) for the RS datasets, the NoAssim case, and
 510 the Best CSO simulation. In WY2017 (Figure 8a), when the NoAssim case overestimates snow depths, the Best CSO simulation
 511 ECDF shifts left, towards the RS dataset ECDF. To a greater degree, in WY2018 (Figure 8c) when the NoAssim case more broadly
 512 overestimates the snow depths, the Best CSO simulation ECDF shifts further left, towards the RS dataset ECDF. The shifts in the
 513 ECDFs are evident in the histograms and the median value of each dataset is indicated with a dashed line (Figure 8b,d). The same
 514 shifts are evident in the snow depth distribution maps (Figure 7c,d,e,f). Even though the shifts in ECDFs and histograms are in the
 515 correct direction in the Best CSO simulations, SnowAssim is not adjusting the distribution of snow depth values, which can be
 516 seen in the multimodal shape of the histograms.

517



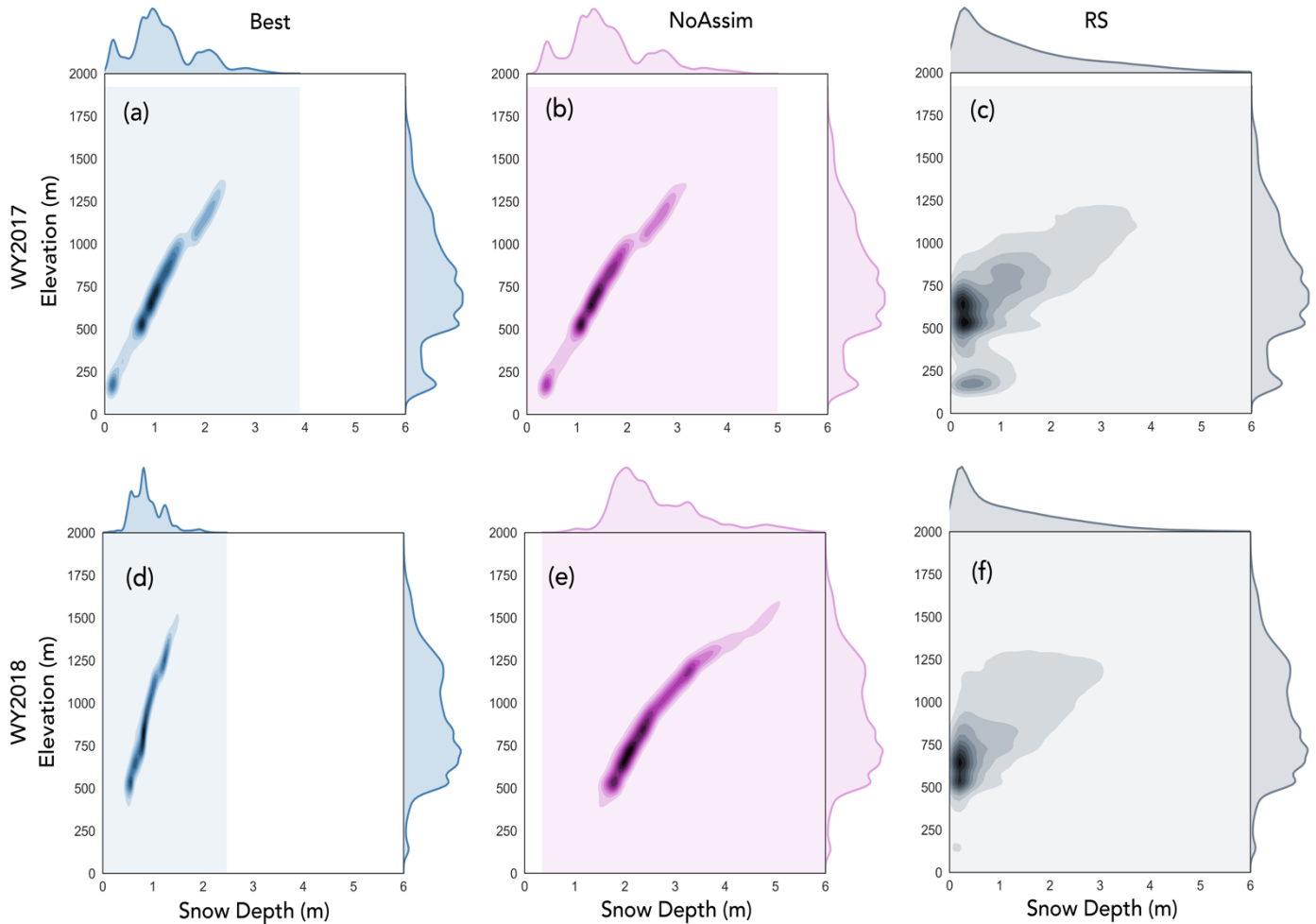
518

519 **Figure 8: Histogram and Distribution Plots.**
 520 **The empirical cumulative distribution functions (ECDFs) and histograms from the best CSO simulation, the no assimilation case, and**
 521 **the remote sensing (RS) datasets during WY2017 (a,b) and WY2018 (c,d).**

522

523 The multimodal distribution of snow depths in the modeled results can be explained by their relationship to the elevation of the
 524 surrounding terrain. The input DEM and the snow depth distributions were compared on a grid-cell-to-grid-cell basis using a two-
 525 dimensional histogram (2DH). Figure 9 is a series of 2DHs that display snow depth (x axes) versus the input DEM (y axes) in the
 526 RS area from both years. Darker colors indicate a higher frequency of snow depth and elevation values corresponding to each
 527 dataset. The 2DHs show a proportional relationship between the modeled snow depths (Figure 9a,b,e,f) and the input DEM values.
 528 As elevation increases, snow depth also increases linearly in the modeled results. Still, the range of snow depths from Best CSO

529 simulation shifts towards the RS dataset in both years, but the elevation relationship remains largely intact. The RS snow depths
 530 are less dependent on elevation, with snow depth values between 0 and 1 appearing at all elevations between 0 and 1250m. The
 531 2DH analysis supports the findings from the snow depth distribution maps where the variability of snow depth observed in the RS
 532 dataset is not replicated in the NoAssim case or the Best CSO simulation (Figure 7).
 533

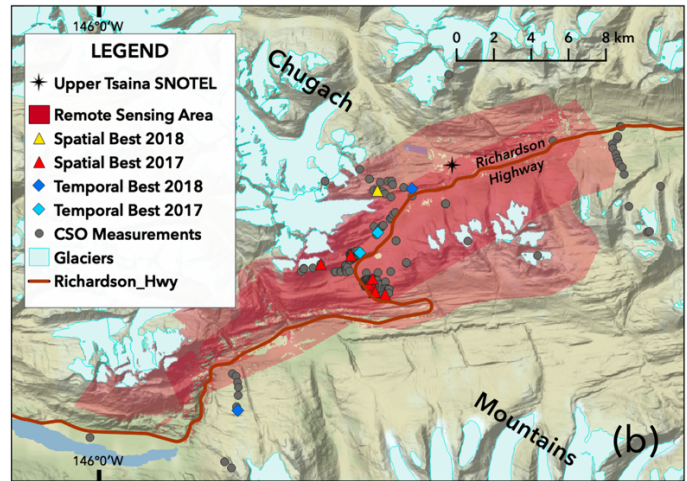
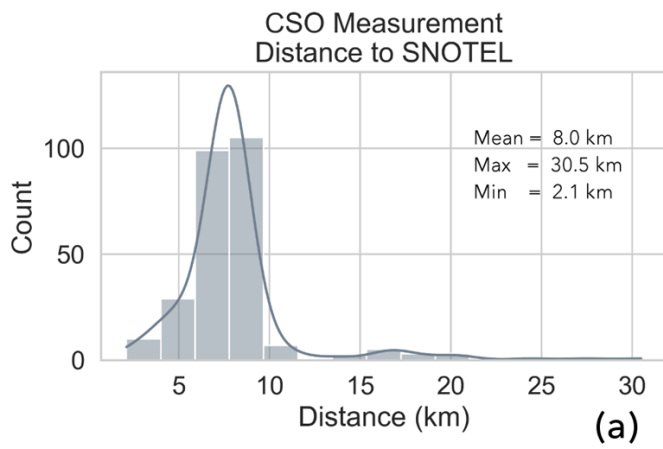


534
 535 **Figure 9: Two-dimensional Histograms.**
 536 **The remote sensing (RS) dataset vs. the (a) water year (WY) 2017 no assimilation case, (b) WY2018 no assimilation case, (c) WY2017**
 537 **best CSO simulation, and (d) WY2018 best CSO simulation.**

538 **6.3 Spatial and Temporal Characteristics of the Assimilated Data**

539 The geographic locations of the CSO measurements used in the temporal and spatial results are an important factor that can shed
 540 some light on our understanding of the assimilation process. First, the time-series analysis validation metrics were quantified for
 541 all days in the water year at the UTS location. The CSO measurements that were assimilated in 2017 range in distance from 4.1
 542 km to 30.5 km away from the UTS location, while the Best CSO simulation measurements (n=2) were located 5.5 and 6.9 km
 543 away. In 2018 the assimilated measurements range in distance from 2.1 km to 17.4 km away from the UTS location, and the Best
 544 CSO simulation measurements (n=2) were located 9.1 and 17.5 km away. Figure 10 includes a map of the assimilated
 545 measurements and a histogram of the distance between the CSO measurements and the UTS station from both water years,
 546 subset by the assimilation time period (on or after April 15th of each year). This distance analysis demonstrates that the CSO

547 measurements used in the time-series assimilation do not coincide with the SNOTEL grid cell location. The histogram shows
 548 that improvements made at the SNOTEL location during assimilation were due to snow depth measurements taken by CSO
 549 participants kilometers away.
 550



551
 552 **Figure 10: Assimilated measurements.**

553 **(a) A histogram showing the distance between the CSO measurements available for assimilation and the Upper Tsaina SNOTEL**
 554 **station, subset by the assimilation time period, on or after April 15th (n=266). A kernel density estimator is used to smooth the**
 555 **distribution. (b) A map of the CSO measurement locations that includes the best spatial and temporal CSO simulations for both water**
 556 **years. The map is zoomed in on the area of the highest density of CSO measurements.**

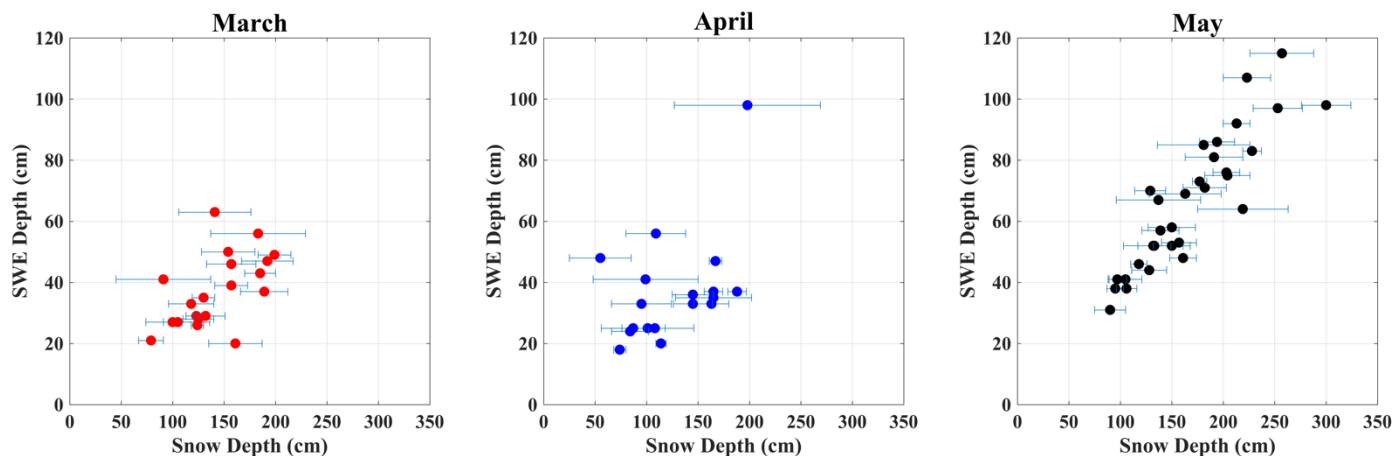
557
 558 Secondly, the remote sensing datasets were collected on April 29th in 2017 and April 7th and 8th in 2018. These validation datasets
 559 are essentially a spatial snapshot of snow depth from a single day in both water years. In water year 2017, there were a total of 9
 560 CSO measurements submitted on April 29th, the same day as the remote sensing dataset collection. For the presented results in
 561 Section 6.2, none of these 9 CSO measurements from April 29th were used. For water year 2018, the remote sensing dataset was
 562 collected on April 8th and the measurements were not assimilated temporally until at least April 15th (see the experimental design
 563 outlined in Section 5). Figure 10b displays the locations of the CSO measurements assimilated in the Best CSO simulation from
 564 both water years (WY2017 n=1; WY2018 n=8). This analysis of the assimilated data demonstrates that the CSO measurements
 565 used in the spatial assimilation do not coincide with the dates of the remote sensing acquisition, revealing that improvements were
 566 made during assimilation by measurements that were taken at a different time.
 567

568 **6.4 2018 Fieldwork Results**

569 To validate the WY2018 SWE distributions from the NoAssim case and the Best CSO simulation we used ground-truth data from
 570 our field campaign in April 2018. The locations of the 70 SWE and snow depth measurement sites from 2018 are depicted in
 571 Figure 1b. Figure 11 shows the co-located SWE depth measurements (y axes) versus the snow depth measurements (x axes) from
 572 each site aggregated by month. The bars in Figure 11 represent the variability in snow depth within the surrounding 100m² of the
 573 SWE measurement, including the average, minimum, and maximum of 8 snow depth measurements at each site. Table 2 shows
 574 the results at the SWE measurement sites, comparing the NoAssim case versus the Best CSO simulation using RMSE, bias, and
 575 mean absolute error (MAE) metrics for evaluation. Since each measurement site corresponds to a single CSO snow depth

576 submission, we separated those measurement sites used in the assimilation scheme from the validation set when creating Table 2.
 577 The Best CSO simulation outperforms the NoAssim case according to all metrics in all months. The 2018 fieldwork results from
 578 April show that the Best CSO simulation has a bias of +3 cm, while the NoAssim case is +97 cm. The April 2018 fieldwork results
 579 agree with the histogram and ECDF analysis that displayed broad overestimation of SWE in the NoAssim case in WY2018 (Figure
 580 7b; Figure 8d).

581
 582 Additionally, we used the co-located snow depth and SWE measurements at the fieldwork sites to quantify the uncertainty that is
 583 added to the model during the snow depth to SWE conversion. By converting the fieldwork snow depth values to SWE using the
 584 Hill et al. (2019) method, we can compare the measured SWE to the approximated SWE values. The fieldwork measured mean
 585 SWE is 51 cm, the RMSE in SWE is 10.5 cm, and the Bias in SWE is 0.6 cm when using the Hill method for all fieldwork sites.
 586



587
 588 **Figure 11: Fieldwork 2018 Measurements by Month**
 589 The 70 *in-situ* snow water equivalent (SWE) measurements (y axes) from 2018 are plotted by month along with their co-located snow
 590 depth measurements (x axes). The bars show the minimum, maximum, and average of each fieldwork site where 8 snow depth
 591 measurements were obtained in a 100 m² area.

592 **Table 2: Fieldwork 2018 Results**
 593 The 70 SWE measurements from the 2018 fieldwork compared to the Best CSO simulation and the no assimilation (NoAssim) case
 594 using the three model performance metrics: root mean squared error (RMSE), mean bias error (Bias), and mean absolute error
 595 (MAE).

	Bias SWE (cm)		RMSE SWE (cm)		MAE SWE (cm)	
	Best CSO	NoAssim	Best CSO	NoAssim	Best CSO	NoAssim
All	-11	86	28	100	22	86
March	-3	77	15	95	13	77
April	3	97	21	114	16	97
May	-25	84	37	95	31	84

596
 597 **6.5 Spatially Averaged Snow Water Equivalent Results**

598 Another way to quantify the ability of CSO measurements to constrain SnowModel output is to investigate the modeled SWE
 599 averaged over a large area. Table 3 contains the spatially averaged SWE estimations from the RS survey area in WY2018, and

600 includes the RS dataset, the Best CSO simulation, and the NoAssim case. We focus on WY2018 because the fieldwork
 601 measurements include estimated bulk density values at each measurement site. These bulk density estimations were measured
 602 during April 2018 and were partitioned from the larger dataset and spatially averaged over the RS region only (n=22). The
 603 fieldwork estimated bulk density value was then applied to the spatially averaged RS snow depth. The uncertainty estimations for
 604 the RS survey dataset and the Federal Sampler collected data are also added to Table 3 to create a range of estimation of water
 605 volume. For the Best CSO simulation and the NoAssim case, the spatially averaged snow depth, SWE, and snow density values
 606 were taken directly from the model results. The SWE estimation results in Table 3 demonstrate that SnowAssim can constrain the
 607 SWE output over a large region based on a few, randomly chosen CSO measurements. Importantly, the accuracy of the total
 608 modeled water volume from the RS region in 2018 improves when CSO measurements are included, a key finding that has
 609 implications for water resource management decisions in snowy, data-limited, mountain environments.

610

611 **Table 3: Spatially Averaged Variables in the RS Region**
 612 **The spatially averaged results were calculated using the RS region in WY2018, the RS dataset (± 1 cm error), the spatially averaged**
 613 **density, and the modeled results. The spatially averaged SWE depth for the RS survey was estimated using the average density (\pm**
 614 **11.2%) measured during April 2018 fieldwork.**

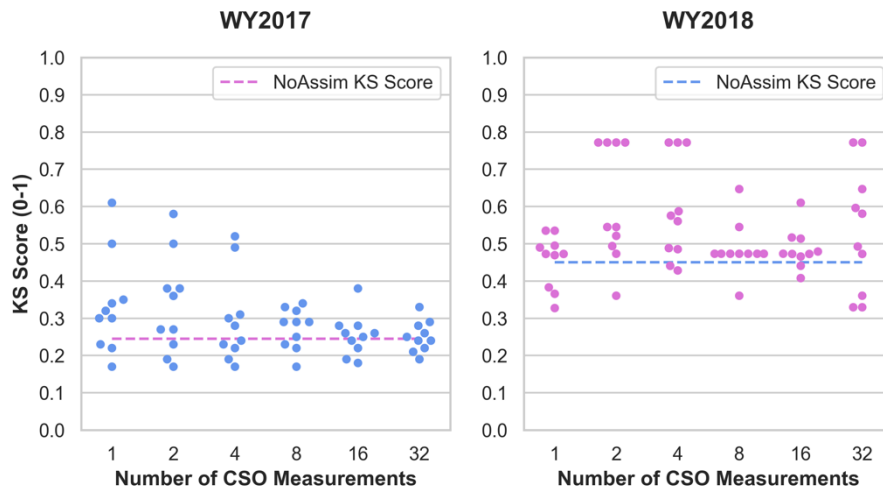
Dataset	Spatially Averaged Snow Depth (cm)	Spatially Averaged Density (kg/m ³)	Spatially Averaged SWE Depth (cm)	Total RS Region Water Volume (km ³)
RS Survey 2018	130 \pm 1 (RS survey)	331 \pm 37 (fieldwork)	38 - 48 (estimated)	0.06 – 0.07 (estimated)
Best CSO Simulation 2018	130 (modeled)	400 (modeled)	52 (modeled)	0.08 (modeled)
NoAssim 2018	267 (modeled)	430 (modeled)	115 (modeled)	0.17 (modeled)

615

616 6.6 Precipitation Adjustment Experiment

617 The experimental design of the present study was developed for remote locations where a long-term precipitation dataset was not
 618 available to bias correct the precipitation inputs. However, since a long-term precipitation dataset may be available in other
 619 locations, we decided to test the results with a precipitation experiment. In this experiment we applied a scalar to the CFSv2
 620 precipitation fields for bias correction and all other model parameters and input datasets were held constant. The experiment results
 621 show that some of the CSO ensemble simulations still outperformed the NoAssim case with the precipitation adjustment, both
 622 spatially and temporally. For example, the spatial results show that 43% percent of the ensemble runs in WY2017 and 20% of the
 623 ensemble runs in WY2018 outperformed the NoAssim case when the precipitation was bias corrected, according to their KS score
 624 (Figure 12). Similarly, the temporal results show that 42% of the ensemble runs in WY2017 and 58% of the ensemble runs in
 625 WY2018 outperformed the NoAssim case when the precipitation was bias corrected, according to their KGE score. The ECDF
 626 and histogram analysis from the precipitation adjustment factor experiment also show model improvements when there was broad
 627 underestimation of snow depths in the NoAssim case in WY2017 and broad overestimation in WY2018. These results demonstrate
 628 that using CSO measurements for assimilation can improve model performance when the available weather forcing dataset has
 629 known biases (no precipitation adjustment factor case) but when those biases have been decreased (precipitation adjustment factor
 630 case) the improvements become less clear, they vary from year to year, and are less consistent between spatial and temporal results.

631



632

633

634

635

636

637

638

6.7 Correction Factor Results

639

640

641

642

643

644

645

646

647

648

649

650

SnowAssim generates a set of correction factors for each of the CSO ensemble member simulations. These factors correspond to the observed and measured differences in the SWE variable and are used to create a correction surface with the Barnes objective analysis. Table 4 reviews a subset of the correction factors, including data from the Best ranked CSO simulations according to the various temporal and spatial metrics previously reviewed in sections 6.1 and 6.2. The number of observations varies for the Best ranked simulation, as well as the precipitation correction factors, the use of a melt correction factor, and whether an interpolated correction surface was created. These correction factor results show that relatively few measurements are needed during assimilation and that there are multiple paths to improving model performance when assimilating CSO observations using SnowAssim.

Table 4: Correction factors from the assimilation scheme for the best ranked simulations from both water years. The model determination for precipitation vs melt correction factors is included and whether the Barnes objective analysis created a spatially distributed correction surface.

Type	Ranking	Year	# of Obs	Precipitation Correction Factors	Melt Correction Factors (-)	Interpolated Surface?	Dates
Temporal	Best	2017	2	0.45, 1.04	n/a	Yes	4/29/17
Temporals	Best	2018	2	0.68, 0.76	n/a	Yes	5/15/18
Spatial	Best	2017	8	0.30, 0.50, 0.73, 0.86, 1.36	6.32, 2.29, 22.6	Yes	4/29/17; 5/8/17
Spatial	Best	2018	1	0.32	n/a	No	5/22/18

651

652 7 Discussion

653 An important consideration in the results of the present study involves ranking the CSO ensemble members by various spatial and
654 temporal metrics. The time series results (Section 6.1), the spatially distributed results (Section 6.2), and the spatially averaged
655 results (Section 6.5) did not have the same ranking order for the CSO ensemble members. For example, the Best CSO simulation
656 in WY2017 from the time-series analysis was an ensemble member with two CSO measurements assimilated according to the
657 KGE metric. The time-series results represent a single point in the domain at the UTS station. By contrast, the Best CSO simulation
658 in WY2017 from the spatial distribution analysis was an ensemble member with eight CSO measurements assimilated using the
659 KS score. The spatially distributed results represent the entire RS survey area. The improvements in model performance are
660 determined by the type of validation dataset available and the metric used to quantify those improvements. In other words, one
661 size does not fit all when it comes to quantifying improvements to model performance using CSO measurements.

662
663 The variability of snow depth and SWE in mountain catchments and the spatial patterning of snowpack conditions in complex
664 terrain is a well-known challenge in snow modeling and snow remote sensing research (Anderton et al., 2004; López-Moreno et
665 al., 2013; Luce et al., 1998; Molotch et al., 2005; Rice and Bales, 2010; Sturm and Wagner, 2010b). The RS results reveal that
666 variability in snow depth across short distances is largely a function of wind redistribution and drifting and not primarily a function
667 of elevation (Figure 8c,f; Figure 6a,b). Thompson Pass is a notoriously windy location, and the RS dataset shows complex drifting
668 patterns throughout the surveyed area (Figure 6a,b). The wind inputs from the reanalysis product used in Micromet and
669 SnowTran3d may not be adequate for the steepness and ruggedness of the terrain. Although wind scaling factors were tested in the
670 calibration, the only suitable calibration dataset was the SNOTEL site. SNOTEL stations are often situated in locations where the
671 effects of wind redistribution of the snowpack are minimal and SNOTEL station data are often not representative of the spatial
672 variability of the surrounding areas (Dressler et al., 2006; Molotch and Bales, 2005). The inability of SnowTran3d to resolve the
673 wind redistribution of the snowpack more accurately, the coarse wind field inputs from the reanalysis products, and the use of a
674 single SNOTEL station for calibration, together represent a model and input data limitation of the current study.

675
676 The ensemble results highlight a broader issue in snow hydrology and process modeling in general, regarding the sub-grid scale
677 variability of the modeled state variable within a single model grid cell. The scale of the *in-situ* observations (measured with an
678 avalanche probe) and the scale of the model resolution (30 m grid) versus the scale of the physical process being modeled (true
679 patterns and true variance in space and time) can create scale effects that need to be accounted for (Blöschl et al., 1999). In this
680 way, the 2018 fieldwork has a significant role to play in our understanding of the sub-grid scale variability in snow depth
681 distributions. CSO participants average a few point measurements over a 1 to 4 m² area. The model resolution is 30 m, or 900 m²
682 per grid model grid cell. If participants move slightly one direction or another, their averaged and submitted measurements would
683 likely be different, but their measurements would potentially lie within the same 30 m model grid cell. This difference, in turn,
684 would modify the SWE depth inputs for SnowAssim. To better characterize the sub-grid scale variability of snow depth we
685 investigate the 8 avalanche probe depths taken over 100 m² at each of the 70 observation sites during the 2018 fieldwork (see also
686 Figure 11). From these data, a picture of the sub-grid scale variability emerges. The largest range in snow depth values at a single
687 100 m² observation site is 2.11 m and the smallest range in snow depth values at a single site is 0.09 m. The highest standard
688 deviation (sd) found at a single observation site is 0.71 m and the lowest sd is 0.04 m. This shows that a significant amount of
689 variation, and therefore uncertainty, is being added to the model chain simply by the sub-grid scale variability of snow depth

690 distributions within a single model grid cell, distributions that the model will not be able to resolve at the low model spatial
691 resolution. Sub-grid scale variability is a well known problem in snow science and represents a limitation of the improvements that
692 can be made by assimilating CSO measurements (Blöschl and Kirnbauer, 1993; Elder et al., 1998; Liston and Hiemstra, 2008;
693 Schmucki et al., 2013).

694

695 One of the limitations of the present study is that the physical and temporal characteristics of the CSO measurements like aspect,
696 elevation, and early-season measurements were not fully analyzed. Initial simulations demonstrated that SnowAssim performs best
697 when the assimilated measurements were located close in time to the validation dataset. This factor influenced our choice to focus
698 on the late-season time period of CSO measurements since the RS surveys were conducted in the late-season. Additionally, since
699 the majority of the CSO measurements for both WYs occurred between March 15th and May 15th, future research should be in a
700 location where CSO measurements are obtained frequently throughout the accumulation season. A research project with many
701 measurements throughout the accumulation period may provide more insights into the temporal aspects of assimilation of CSO
702 measurements. We decided not to subset the CSO measurements by geophysical characteristics like aspect, elevation, and land
703 cover type because these require additional analysis that is outside of the scope of the current study. Understanding the effects of
704 temporal and spatial restrictions of CSO measurements on model performance will likely be an area of future research.
705 Additionally, it may be necessary to test other process models and alternate assimilation schemes in the future to improve the
706 spatial distribution of model results and determine if CSO measurements can be used in other modeling contexts.

707

708 **8 Conclusions**

709 In this study we use a new snow dataset collected by participants in the Community Snow Observations (CSO) project in coastal
710 Alaska to improve snow depth and snow water equivalence (SWE) outputs from a snow process model. Ensemble simulations
711 were carried out during the 2017 and 2018 snow seasons to investigate the effects of incorporating citizen science measurements
712 into the model chain using an assimilation scheme. Time series SNOTEL station records, remotely sensed photogrammetry and
713 light detection and ranging surveys, and fieldwork observations are used to validate the modeled snow depth and snow water
714 equivalent distributions. Any number of CSO measurements assimilated improves model performance, from 1 to 32. Our results
715 demonstrate that using CSO measurements for assimilation can improve model performance when the available weather forcing
716 dataset has known biases and also when those biases have been decreased by using a precipitation adjustment factor. The
717 improvements in model performance from CSO measurements occur in 62% to 78% of the ensemble simulations both spatially
718 and temporally, and in cases when the model broadly overestimates or underestimates snow depth and SWE. Model estimations
719 of total water volume from a sub-region of the study area also demonstrate improvements in accuracy after CSO measurements
720 have been assimilated. This study has implications for water resource management and snow modeling in locations where *in-situ*
721 snow information is limited but snow enthusiasts often visit, since even small numbers of assimilated CSO measurements can
722 improve the snow model outputs.

723

724

726 **Appendix A: Model calibration parameters and their descriptions.**

Parameter	# of Options	Format	Description
Temperature Lapse Rate	3 sets	Monthly	PRISM Climatologies; Local Weather Station Data; SnowModel Default
Precipitation Lapse Rate	5 sets	Monthly	Monthly Coefficients of 1/4, 1/2, 3/4, 1 (SnowModel Default), PRISM Climatologies
Wind Adjustment Factor	3	Coefficient	Coefficients of 1 (SnowModel Default), 2, 3
SnowTran3d	2	On/Off	

727

728

729 **Appendix B: Top performing parameter configurations from the calibration simulations.**

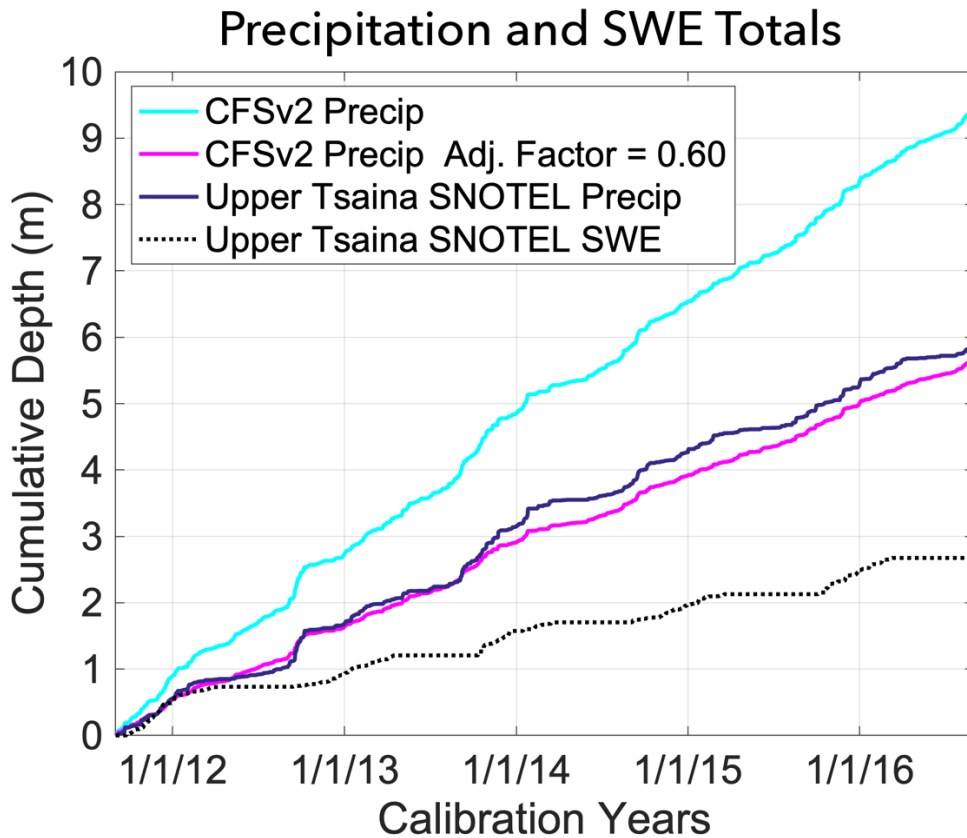
Rank	Temperature Lapse Rate	Precipitation Scaling Factor	Wind Adjustment Factor	SnoTran on/off
Tied for first	Default	Default	Default	On
Tied for first	Local Weather Station	Default	Default	On
Tied for first	PRISM Climatologies	Default	Default	On

730

731

732

733 **Appendix C: Precipitation totals at the Upper Tsaina SNOTEL station compared to the CFSv2-forced model totals and the CFSv2-**
 734 **forced model totals with a precipitation adjustment factor. This overestimation of precipitation by the reanalysis product is a major**
 735 **factor in the quality of the calibration results.**



736

737
738
739
740

Appendix D: Precipitation Adjustment Factor Results.

The best precipitation adjustment factors are shown, along with the root mean squared error (RMSE), the Nash Sutcliffe Efficiency (NSE), the Kling-Gupta Efficiency (KGE), and the mean bias error (Bias).

Reanalysis, Resolution	Time	Time Step	Number of Simulations	Precipitation	RMSE			Bias
	Period (WY)			Adjustment Factor	Precipitation (mm)	NSE	KGE	Precipitation (+/- mm)
MERRA2, 30m	2012-2016	3hrly	11	0.55	7.5	0.07	0.20	0.0
MERRA2, 100m	2012-2016	3hrly	11	0.55	7.5	0.07	0.20	0.0
CFSv2, 30m	2012-2016	6hrly	11	0.60	6.7	0.27	0.35	-0.1
CFSv2, 100m	2012-2016	6hrly	11	0.60	6.7	0.27	0.35	-0.1

741
742
743
744
745

Appendix E: Ranked Temporal Results.

Ensemble results from ranked by Kling-Gupta efficiency (KGE) score for water year (WY) 2017 (a) and WY2018 (b). Also included are the Nash Sutcliffe Efficiency (NSE) and the mean bias error (Bias) values.

(a) WY2017

Rank	Number of CSO Measurements	Iteration	KGE	NSE	Bias (cm)
1	2	2	0.97	0.99	0
2	1	8	0.97	0.99	0
3	4	1	0.94	0.93	0
4	2	6	0.93	0.92	0
5	8	9	0.93	0.89	-1
6	16	8	0.90	0.84	-1
7	32	3	0.88	0.96	-1
8	4	4	0.88	0.91	-2
9	1	10	0.80	0.95	-3
10	4	3	0.80	0.89	2
11	16	2	0.78	0.82	-3
12	8	1	0.77	0.81	2
13	32	8	0.77	0.79	-3
14	2	8	0.77	0.93	-3
15	16	7	0.76	0.93	-3
16	16	1	0.75	0.87	-3
17	4	6	0.74	0.92	-3
18	1	6	0.71	0.89	4
19	16	3	0.67	0.88	-4
20	32	4	0.66	0.79	-5
21	32	5	0.65	0.78	-5
22	32	1	0.65	0.78	-5
23	32	7	0.64	0.80	-5
24	2	3	0.63	0.80	4
25	4	9	0.62	0.83	-5
26	16	9	0.62	0.82	-5
27	2	10	0.61	0.82	-5
28	16	4	0.60	0.75	-5
29	32	6	0.59	0.82	-5
30	8	8	0.59	0.76	5
31	32	2	0.57	0.78	6
32	16	5	0.56	0.73	-6
33	4	8	0.56	0.73	-6

746

34	8	10	0.55	0.72	-6
35	8	7	0.54	0.73	-6
36	16	6	0.54	0.70	-6
37	1	3	0.54	0.74	6
38	8	2	0.52	0.68	-6
39	8	4	0.52	0.71	-6
40	1	2	0.51	0.72	-6
41	4	10	0.50	0.67	-7
42	32	10	0.49	0.66	-7
43	4	7	0.46	0.63	-7
NoAssim	NoAssim	NoAssim	0.47	0.66	7
44	8	3	0.43	0.66	-7
45	32	9	0.41	0.63	-8
46	8	5	0.39	0.54	-8
47	2	1	0.36	0.53	-8
48	8	6	0.34	0.49	-9
49	1	4	0.33	0.49	-9
50	1	7	0.29	0.42	-9
51	2	4	0.28	0.41	-9
52	16	10	0.26	0.37	-10
53	2	5	0.22	0.32	-10
54	1	5	0.17	0.23	-11
55	1	9	0.08	0.05	-12
56	2	7	0.08	0.05	-12
57	4	2	0.06	0.02	-12
58	4	5	0.03	-0.03	-12
59	2	9	-0.02	-0.13	-13
60	1	1	-0.07	-0.24	-14

747

748

(b) WY2018

Rank	Number of CSO Measurements	Iteration	KGE	NSE	Bias (m)
1	2	7	0.95	0.96	0
2	8	9	0.91	0.90	2
3	8	5	0.90	0.89	2
4	2	9	0.88	0.91	2
5	2	4	0.87	0.93	-2
6	4	7	0.87	0.97	3
7	4	8	0.84	0.97	-2
8	1	5	0.84	0.95	-2
9	1	6	0.84	0.95	-2
10	4	10	0.82	0.95	4
11	2	2	0.77	0.92	5
12	4	9	0.77	0.88	-4
13	16	9	0.76	0.85	-4
14	16	5	0.76	0.53	-2
15	16	4	0.76	0.53	-2
16	4	6	0.75	0.84	-4
17	32	10	0.74	0.49	-2
18	4	5	0.71	0.72	-5
19	2	6	0.71	0.89	6
20	1	8	0.71	0.83	-5
21	1	1	0.71	0.83	-5
22	1	9	0.71	0.83	-5
23	8	7	0.69	0.80	-6
24	16	8	0.68	0.58	-6
25	16	2	0.65	0.77	-6
26	32	2	0.65	0.53	-6
27	32	5	0.64	0.50	-6
28	32	8	0.64	0.49	-6
29	32	7	0.62	0.47	-6

30	32	9	0.62	0.47	-6
31	32	4	0.62	0.46	-6
32	32	1	0.62	0.46	-6
33	8	10	0.57	0.42	-7
34	4	1	0.53	0.65	-9
35	2	1	0.52	0.65	-9
36	32	3	0.49	0.18	6
37	4	4	0.48	0.60	-10
38	4	2	0.47	0.60	-10
39	4	3	0.45	0.57	-10
40	8	6	0.43	0.52	11
41	2	3	0.38	0.46	-11
42	1	7	0.33	0.38	-12
43	8	4	0.30	0.29	-13
44	1	2	0.30	0.36	15
45	16	1	0.24	0.14	-14
46	32	6	0.24	0.13	-14
47	1	4	0.23	0.29	16
48	1	10	0.07	-0.09	-17
49	8	8	0.01	-0.21	-18
50	8	3	0.00	-0.24	-18
51	1	3	-0.07	-0.37	-20
52	16	3	-0.15	-1.18	18
53	16	7	-0.16	-1.15	18
54	16	6	-0.16	-1.15	18
55	8	1	-0.16	-1.14	18
56	16	10	-0.16	-1.13	19
57	2	8	-0.23	-1.05	21
58	8	2	-0.28	-1.07	23
59	2	5	-0.37	-1.18	27
60	2	10	-0.58	-2.00	32

749

750

751

752

753

754

Appendix F: Ranked Spatial Results.

Spatial distribution ensemble results ranked by Kolmogorov-Smirnov (KS) score for water year (WY) 2017 (a) and WY2018 (b). Also included are the root mean squared error (RMSE) and the median values.

(a) WY2017 Results

Rank	Number of CSO Measurements	Iteration	KS Score (0 - 1)	RMSE (m)	Median (m)	Mean (m)
1	8	9	0.17	1.171	1.071	1.198
2	1	8	0.17	1.173	1.066	1.192
3	2	2	0.17	1.173	1.064	1.190
4	4	1	0.18	1.164	1.096	1.225
5	2	6	0.19	1.159	1.116	1.248
6	4	4	0.19	1.202	0.983	1.100
7	32	2	0.21	1.149	1.156	1.393
8	32	3	0.21	1.222	0.931	1.044
9	8	8	0.21	1.148	1.166	1.402
10	1	10	0.22	1.243	0.888	0.995
11	16	8	0.22	1.287	0.693	0.883
12	16	1	0.23	1.251	0.872	0.978
13	2	8	0.23	1.256	0.861	0.966
14	4	2	0.23	1.135	1.250	1.396
15	4	3	0.23	1.135	1.250	1.396
16	4	6	0.24	1.267	0.840	0.942
17	16	7	0.24	1.270	0.834	0.936
18	8	1	0.24	1.133	1.281	1.430
19	1	6	0.24	1.133	1.281	1.430
20	16	2	0.25	1.321	0.651	0.814
21	32	4	0.25	1.293	0.801	0.891

22		32	5	0.25	1.293	0.794	0.892
23		16	3	0.26	1.306	0.770	0.866
24		32	1	0.26	1.310	0.761	0.855
25		32	7	0.27	1.316	0.754	0.847
26		4	9	0.27	1.320	0.749	0.843
27		16	4	0.27	1.324	0.738	0.832
28		2	10	0.27	1.328	0.731	0.825
29		16	9	0.27	1.328	0.730	0.824
30		2	3	0.27	1.135	1.406	1.567
31		8	10	0.28	1.344	0.715	0.804
32		1	3	0.28	1.137	1.426	1.589
33		16	5	0.28	1.349	0.696	0.788
34		4	8	0.29	1.350	0.694	0.786
35		32	6	0.29	1.351	0.692	0.784
36		16	6	0.29	1.355	0.685	0.777
37		8	7	0.29	1.360	0.678	0.769
NoAssim	NoAssim	NoAssim	NoAssim	0.30	1.145	1.482	1.651
38		8	2	0.30	1.370	0.663	0.753
39		32	10	0.30	1.384	0.649	0.731
40		1	2	0.30	1.381	0.644	0.734
41		4	10	0.30	1.384	0.639	0.729
42		32	8	0.31	1.404	0.461	0.667
43		8	4	0.31	1.400	0.614	0.703
44		4	7	0.32	1.402	0.612	0.701
45		8	3	0.33	1.426	0.573	0.662
46		8	5	0.34	1.438	0.565	0.649
47		32	9	0.34	1.448	0.546	0.630
48		8	6	0.35	1.469	0.521	0.603
49		2	1	0.36	1.468	0.514	0.600
50		1	4	0.37	1.484	0.490	0.576
51		1	7	0.38	1.510	0.453	0.539
52		2	4	0.38	1.510	0.453	0.539
53		16	10	0.39	1.529	0.426	0.512
54		2	5	0.41	1.559	0.385	0.472
55		1	5	0.44	1.601	0.330	0.418
56		1	9	0.50	1.684	0.223	0.314
57		2	7	0.50	1.684	0.223	0.314
58		4	5	0.53	1.724	0.175	0.268
59		2	9	0.57	1.770	0.119	0.217
60		1	1	0.61	1.812	0.067	0.173

755

756

757

758

759

(b) WY2018 Results

Rank	Number of CSO Measurements	Iteration	KS Score (0 - 1)	RMSE (m)	Median (m)	Mean (m)
1	1	10	0.30	1.210	0.838	0.905
2	8	3	0.34	1.246	0.756	0.810
3	8	8	0.34	1.246	0.756	0.810
4	1	7	0.38	1.146	1.124	1.238
5	16	1	0.38	1.150	1.127	1.237
6	32	6	0.38	1.150	1.127	1.237
7	8	4	0.38	1.150	1.127	1.237
8	2	3	0.39	1.146	1.182	1.304
9	1	3	0.41	1.319	0.621	0.655
10	4	3	0.41	1.153	1.261	1.392
11	4	1	0.42	1.147	1.292	1.437
12	4	2	0.42	1.155	1.279	1.413
13	4	4	0.42	1.165	1.305	1.435

14	2	1	0.43	1.166	1.335	1.474
15	8	7	0.46	1.205	1.487	1.651
16	16	2	0.47	1.261	1.568	1.708
17	1	1	0.47	1.221	1.521	1.684
18	1	9	0.47	1.221	1.521	1.684
19	1	8	0.47	1.221	1.523	1.686
20	16	8	0.48	1.233	1.553	1.746
21	32	1	0.48	1.233	1.553	1.746
22	32	2	0.48	1.233	1.553	1.746
23	32	4	0.48	1.233	1.553	1.746
24	32	5	0.48	1.233	1.553	1.746
25	32	7	0.48	1.233	1.553	1.746
26	32	8	0.48	1.233	1.553	1.746
27	32	9	0.48	1.233	1.553	1.746
28	4	9	0.48	1.244	1.577	1.753
29	4	5	0.48	1.248	1.580	1.748
30	4	6	0.48	1.248	1.580	1.748
31	1	5	0.49	1.259	1.607	1.780
32	1	6	0.49	1.259	1.607	1.780
33	4	8	0.49	1.259	1.607	1.780
34	8	10	0.49	1.259	1.607	1.780
35	16	9	0.49	1.281	1.628	1.801
36	2	4	0.51	1.318	1.714	1.893
37	2	7	0.53	1.353	1.777	1.968
38	16	4	0.54	1.401	1.848	2.068
39	16	5	0.54	1.401	1.848	2.068
40	32	10	0.54	1.401	1.848	2.068
41	8	9	0.55	1.453	1.922	2.131
42	4	7	0.55	1.454	1.928	2.132
43	2	9	0.56	1.461	1.939	2.148
44	8	5	0.56	1.500	1.977	2.189
45	4	10	0.56	1.493	1.980	2.191
46	2	2	0.58	1.540	2.043	2.263
47	2	6	0.59	1.606	2.128	2.350
NoAssim	NoAssim	NoAssim	0.64	1.861	2.411	2.678
48	1	2	0.65	1.894	2.436	2.721
49	32	3	0.65	1.928	2.466	2.764
50	8	6	0.65	1.928	2.466	2.764
51	1	4	0.66	2.009	2.567	2.852
52	16	10	0.77	2.932	3.466	3.839
53	16	3	0.77	2.932	3.466	3.839
54	16	6	0.77	2.932	3.466	3.839
55	16	7	0.77	2.932	3.466	3.839
56	2	10	0.77	2.932	3.466	3.839
57	2	5	0.77	2.932	3.466	3.839
58	2	8	0.77	2.932	3.466	3.839
59	8	1	0.77	2.932	3.466	3.839
60	8	2	0.77	2.932	3.466	3.839

760

761 **10 Code and Data Availability**

762 The datasets used in this study can be found at the following locations.

763

- 764 1. Community Snow Observations website and snow depth data download at <http://app.communitysnowobs.org/>
765 (last accessed 30 April 2020).

766

- 767 2. The snow depth to snow water equivalence calculator (Hill et al., 2019) can be downloaded via Github at
768 <https://github.com/communitysnowobs/snowdensity> (last accessed: 30 April 2020).
769
- 770 3. Snow Telemetry data for the Upper Tsaina River station near Valdez, Alaska is available at the Natural Resources
771 Conservation Service website: <https://wcc.sc.egov.usda.gov/nwcc/site?sitenum=1055> (last accessed: 30 April 2020).
772
- 773 4. Climate Forecast System Reanalysis version 2 (CFSv2) data (Saha et al., 2011) is available for download at
774 <https://rda.ucar.edu/datasets/ds094.0/#!/description>.
775
- 776 5. The CFSv2 data was accessed using Google Earth Engine at [https://developers.google.com/earth-
777 engine/datasets/catalog/NOAA_CFSV2_FOR6H](https://developers.google.com/earth-engine/datasets/catalog/NOAA_CFSV2_FOR6H) (last accessed: 30 April 2020). A javascript version of the Earth Engine
778 code written for this project is available at https://github.com/snowmodel-tools/preprocess_javascript (last accessed: 30
779 April 2020).
780
- 781 6. To convert the CFSv2 data downloaded from Google Earth Engine to the necessary input file for MicroMet we
782 wrote Matlab scripts that can be downloaded via Github at https://github.com/snowmodel-tools/preprocess_matlab (last
783 accessed: 30 April 2020).
784
- 785 7. The MERRA2 weather reanalysis product from NASA's Global Modeling and Assimilation office (Gelaro et
786 al., 2017) can be downloaded at https://gmao.gsfc.nasa.gov/reanalysis/MERRA-2/data_access/ (last accessed: 30 April
787 2020).
788
- 789 8. The National Elevation Dataset is (Gesch et al., 2002) available for download at
790 <https://catalog.data.gov/dataset/usgs-national-elevation-dataset-ned> (last accessed: 30 April 2020).
791
- 792 9. The National Land Cover Database 2011 dataset (Homer et al., 2011) is available for download at the Multi-
793 Resolution Land Characteristics Consortium at <https://www.mrlc.gov/data?f%5B0%5D=category%3Aland%20cover>
794 (last accessed: 30 April 2020).

795 **11 Author Contributions**

796 Ryan Crumley, David Hill, Gabriel Wolken, Katreen Wikstrom Jones, and Anthony Arendt designed the research questions and
797 decided on the methods. Ryan Crumley, Gabriel Wolken, Katreen Wikstrom Jones, Christopher Cosgrove, and David Hill
798 conducted fieldwork in the study area, including snowpack sampling and remote sensing surveys. Ryan Crumley and Dave Hill
799 oversaw the analysis of the manuscript. Anthony Arendt designed and maintained the CSO website and snow dataset with
800 contributions from all authors. Community Snow Observation Participants and all authors contributed snow depth measurements.
801 Ryan Crumley prepared the manuscript with contributions from all authors during editing and review process.

802 **12 Competing Interests**

803 The authors declare that they have no conflicts of interest.

804 **13 Acknowledgements**

805 This research has been supported by NASA (grant no. NNX17AG67A) and CUAHSI (Pathfinder Fellowship grant). Arendt was
806 partially supported by the Washington Research Foundation, and by a Data Science Environments project award to the University
807 of Washington eScience Institute from the Gordon and Betty Moore and the Alfred P. Sloan Foundations. Los Alamos National
808 Laboratory has approved the dissemination of this manuscript with the assigned the LA-UR-21-26394 number.
809

810 **References**

811 Anderton, S.P., White, S.M. and Alvera, B.: Evaluation of spatial variability in snow water equivalent for a high mountain
812 catchment. *Hydrological Processes*, 18(3), pp.435-453, <https://doi.org/10.1002/hyp.1319>, 2004.

813
814 Bales, R.C., Molotch, N.P., Painter, T.H., Dettinger, M.D., Rice, R. and Dozier, J.: Mountain hydrology of the western United
815 States. *Water Resources Research*, 42(8), <https://doi.org/10.1029/2005WR004387>, 2006.
816

817 Baba, M., Gascoïn, S., Jarlan, L., Simonneaux, V. and Hanich, L.: Variations of the Snow Water Equivalent in the Ourika
818 Catchment (Morocco) over 2000–2018 Using Downscaled MERRA-2 Data. *Water*, 10(9), p.1120,
819 <https://doi.org/10.3390/w10091120>, 2018.

820
821 Barnes, S.L.: A technique for maximizing details in numerical weather map analysis, *Journal of Applied Meteorology*, 3(4),
822 pp.396-409, [https://doi.org/10.1175/1520-0450\(1964\)003<0396:ATFMDI>2.0.CO;2](https://doi.org/10.1175/1520-0450(1964)003<0396:ATFMDI>2.0.CO;2), 1964.

823
824 Barnes, S.L.: Mesoscale objective map analysis using weighted time-series observations, Technical Report, National Severe
825 Storms Lab., Norman, Oklahoma, 1973.
826

827 Barnett, T.P., Adam, J.C. and Lettenmaier, D.P.: Potential impacts of a warming climate on water availability in snow-dominated
828 regions. *Nature*, 438(7066), p.303, <https://doi.org/10.1038/nature04141>, 2005.

829
830 Beamer, J.P., Hill, D.F., Arendt, A. and Liston, G.E.: High-resolution modeling of coastal freshwater discharge and glacier mass
831 balance in the Gulf of Alaska watershed, *Water Resources Research*, 52(5), pp.3888-3909,
832 <https://doi.org/10.1002/2015WR018457>, 2016.

833
834 Beamer, J.P., Hill, D.F., McGrath, D., Arendt, A. and Kienholz, C.: Hydrologic impacts of changes in climate and glacier extent
835 in the Gulf of Alaska watershed, *Water Resources Research*, 53, pp.7502-7520, <https://doi.org/10.1002/2016WR020033>, 2017.

836
837 Blöschl, G., Kirnbauer, R.: An analysis of snow cover patterns in a small alpine catchment, *Hydrological Processes*, 6(1), pp.99-
838 109, <https://doi.org/10.1002/hyp.3360060109>, 1992.

839
840 Blöschl, G.: Scaling issues in snow hydrology. *Hydrological processes*, 13(14-15), pp.2149-2175,
841 [https://doi.org/10.1002/\(SICI\)1099-1085\(199910\)13:14/15<2149::AID-HYP847>3.0.CO;2-8](https://doi.org/10.1002/(SICI)1099-1085(199910)13:14/15<2149::AID-HYP847>3.0.CO;2-8), 1999.

842

843 Bohr, G.S. and Aguado, E.: Use of April 1 SWE measurements as estimates of peak seasonal snowpack and total cold-season
844 precipitation. *Water Resources Research*, 37(1), pp.51-60, <https://doi.org/10.1029/2000WR900256>, 2001.

845

846 Bonney, R., Cooper, C.B., Dickinson, J., Kelling, S., Phillips, T., Rosenberg, K.V. and Shirk, J.: Citizen science: a developing tool
847 for expanding science knowledge and scientific literacy. *BioScience*, 59(11), pp.977-984, <https://doi.org/10.1525/bio.2009.59.11.9>,
848 2009.

849

850 Bühler, Y., Adams, M.S., Bösch, R. and Stoffel, A.: Mapping snow depth in alpine terrain with unmanned aerial systems (UASs):
851 potential and limitations. *The Cryosphere*, 10(3), pp.1075-1088, <https://doi.org/10.5194/tc-10-1075-2016>, 2016.

852

853 Buytaert, W., Zulkafli, Z., Grainger, S., Acosta, L., Alemie, T.C., Bastiaensen, J., De Bièvre, B., Bhusal, J., Clark, J., Dewulf, A.
854 and Foggin, M.: Citizen science in hydrology and water resources: opportunities for knowledge generation, ecosystem service
855 management, and sustainable development. *Frontiers in Earth Science*, 2, p.26, <https://doi.org/10.3389/feart.2014.00026>, 2014.

856

857 Carroll, T., Cline, D., Fall, G., Nilsson, A., Li, L. and Rost, A.: NOHRSC operations and the simulation of snow cover properties
858 for the coterminous US. In *Proc. 69th Annual Meeting of the Western Snow Conf* (pp. 1-14), 2001.

859

860 Carrassi, A., Bocquet, M., Bertino, L. and Evensen, G.: Data assimilation in the geosciences: An overview of methods, issues, and
861 perspectives. *Wiley Interdisciplinary Reviews: Climate Change*, 9(5), p.e535, <https://doi.org/10.1002/wcc.535>, 2018.

862

863 Carter, S., Carter, P. and Levison, J.: Skier triggered surface hoar: A discussion of avalanche involvements during the 2006 Valdez
864 Chugach helicopter ski season. In *Proceedings of International Snow Science Workshop* (pp. 860-867), 2006.

865

866 Clark, M.P., Slater, A.G., Barrett, A.P., Hay, L.E., McCabe, G.J., Rajagopalan, B. and Leavesley, G.H.: Assimilation of snow
867 covered area information into hydrologic and land-surface models. *Advances in water resources*, 29(8), pp.1209-1221,
868 <https://doi.org/10.1016/j.advwatres.2005.10.001>, 2006.

869

870 Clark, M.P., Hendrikx, J., Slater, A.G., Kavetski, D., Anderson, B., Cullen, N.J., Kerr, T., Örn Hreinsson, E. and Woods, R.A.:
871 Representing spatial variability of snow water equivalent in hydrologic and land-surface models: A review. *Water Resources*
872 *Research*, 47(7), <https://doi.org/10.1029/2011WR010745>, 2011.

873

874 Contosta, A.R., Adolph, A., Burchsted, D., Burakowski, E., Green, M., Guerra, D., Albert, M., Dibb, J., Martin, M., McDowell,
875 W.H. and Routhier, M.: A longer vernal window: the role of winter coldness and snowpack in driving spring transitions and lags.
876 *Global change biology*, 23(4), pp.1610-1625, <https://doi.org/10.1111/gcb.13517>, 2017.

877

878 Cooper, C. B., Dickinson J., Phillips, T., and Bonney, R.: Citizen science as a tool for conservation in residential ecosystems.
879 *Ecology and Society* 12(2): 11. URL: <http://www.ecologyandsociety.org/vol12/iss2/art11/> (accessed 05 May 2020), 2007.

880

881 Cosgrove, C.L., Wells, J., Nolin, A.W., Putera, J. and Prugh, L.R.: Seasonal influence of snow conditions on Dall's sheep
882 productivity in Wrangell-St Elias National Park and Preserve. *PloS one*, 16(2), p.e0244787, 2021.

883

884 Crumley, R.L., Hill, D.F., Beamer, J.P. and Holzenthal, E.R.: Seasonal components of freshwater runoff in Glacier Bay, Alaska:
885 diverse spatial patterns and temporal change. *The Cryosphere*, 13(6), pp.1597-1619, <https://doi.org/10.5194/tc-13-1597-2019>,
886 2019.

887

888 Deems, J.S. and Painter, T.H.: Lidar measurement of snow depth: accuracy and error sources. In *Proceedings of the 2006*
889 *International Snow Science Workshop: Telluride, Colorado, USA, International Snow Science Workshop* (pp. 330-338), 2006.

890

891 Dickinson, J.L., Zuckerberg, B. and Bonter, D.N.: Citizen science as an ecological research tool: challenges and benefits. *Annual*
892 *review of ecology, evolution, and systematics*, 41, pp.149-172, <https://doi.org/10.1146/annurev-ecolsys-102209-144636>, 2010.

893

894 Dixon, D. and Boon, S.: Comparison of the SnowHydro snow sampler with existing snow tube designs. *Hydrological Processes*,
895 26(17), pp.2555-2562, <https://doi.org/10.1002/hyp.9317>, 2012.

896

897 Dressler, K.A., Fassnacht, S.R. and Bales, R.C.: A comparison of snow telemetry and snow course measurements in the Colorado
898 River basin. *Journal of hydrometeorology*, 7(4), pp.705-712, <https://doi.org/10.1175/JHM506.1>, 2006.

899

900 Elder, K., Rosenthal, W. and Davis, R.E.: Estimating the spatial distribution of snow water equivalence in a montane watershed.
901 *Hydrological Processes*, 12(10-11), pp.1793-1808, [https://doi.org/10.1002/\(SICI\)1099-1085\(199808/09\)12:10/11<1793::AID-](https://doi.org/10.1002/(SICI)1099-1085(199808/09)12:10/11<1793::AID-HYP695>3.0.CO;2-K)
902 [HYP695>3.0.CO;2-K](https://doi.org/10.1002/(SICI)1099-1085(199808/09)12:10/11<1793::AID-HYP695>3.0.CO;2-K), 1998.

903

904 Fayad, A., Gascoin, S., Faour, G., López-Moreno, J.I., Drapeau, L., Le Page, M. and Escadafal, R.: Snow hydrology in
905 Mediterranean mountain regions: A review. *Journal of Hydrology*, 551, pp.374-396, <https://doi.org/10.1016/j.jhydrol.2017.05.063>,
906 2017.

907

908 Fienen, M.N. and Lowry, C.S.: Social. Water—A crowdsourcing tool for environmental data acquisition. *Computers &*
909 *Geosciences*, 49, pp.164-169, <https://doi.org/10.1016/j.cageo.2012.06.015>, 2012.

910

911 Fletcher, S.J., Liston, G.E., Hiemstra, C.A. and Miller, S.D.: Assimilating MODIS and AMSR-E snow observations in a snow
912 evolution model. *Journal of Hydrometeorology*, 13(5), pp.1475-1492, <https://doi.org/10.1175/JHM-D-11-082.1>, 2012.

913

914 Garnett, R. and Stewart, R.: Comparison of GPS units and mobile Apple GPS capabilities in an urban landscape. *Cartography and*
915 *Geographic Information Science*, 42(1), pp.1-8, <https://doi.org/10.1080/15230406.2014.974074>, 2015.

916

917 Gesch, D., Evans, G., Mauck, J., Hutchinson, J., Carswell Jr., W.J.: *The National Map—Elevation: U.S. Geological Survey Fact*
918 *Sheet 2009-3053*, 2009.

919

920 Gelaro, R., McCarty, W., Suárez, M.J., Todling, R., Molod, A., Takacs, L., Randles, C.A., Darmenov, A., Bosilovich, M.G.,
921 Reichle, R. and Wargan, K.: The modern-era retrospective analysis for research and applications, version 2 (MERRA-2). *Journal*
922 *of Climate*, 30(14), pp.5419-5454, <https://doi.org/10.1175/JCLI-D-16-0758.1>, 2017.

923

924 Haberkorn, A.: *European Snow Booklet – an Inventory of Snow Measurements in Europe*. EnviDat.
925 <https://doi.org/10.16904/envidat.59>, 2019.

926
927 Hall D.K., Riggs G.A., Salomonson V.V.: MODIS/Terra Snow Cover Daily L3 Global 500m Grid, Version 6. Boulder, CO: NASA
928 National Snow and Ice Data Center Distributed Active Archive Center, 2016.
929
930 Han, E., Merwade, V. and Heathman, G.C.: Implementation of surface soil moisture data assimilation with watershed scale
931 distributed hydrological model. *Journal of hydrology*, 416, pp.98-117, <https://doi.org/10.1016/j.jhydrol.2011.11.039>, 2012.
932
933 Hedrick, A.R., Marks, D., Havens, S., Robertson, M., Johnson, M., Sandusky, M., Marshall, H.P., Kormos, P.R., Bormann, K.J.
934 and Painter, T.H.: Direct insertion of NASA Airborne Snow Observatory-derived snow depth time series into the iSnobal energy
935 balance snow model. *Water Resources Research*, 54(10), pp.8045-8063, <https://doi.org/10.1029/2018WR023190>, 2018.
936
937 Helmert, J., Lange, M., Dong, J., De Rosnay, P., Gustafsson, D., Churulin, E., Kurzeneva, E., Müller, R., Trentmann, J., Souverijns,
938 N. and Koch, R.: 1st Snow Data Assimilation Workshop in the framework of COST HarmoSnow ESSEM 1404. *Meteorologische*
939 *Zeitschrift*, 27(4), pp.325-333, <https://doi.org/10.1127/metz/2018/0906>, 2018.
940
941 Hendriks, J., Johnson, J. and Shelly, C.: Using GPS tracking to explore terrain preferences of heli-ski guides. *Journal of outdoor*
942 *recreation and tourism*, 13, pp.34-43, <https://doi.org/10.1016/j.jort.2015.11.004>, 2016.
943
944 Hill, D., Wolken, G., Wikstrom Jones K., Crumley, R., and Arendt, A.: Crowdsourcing snow depth data with citizen scientists,
945 *Eos*, 99, <https://doi.org/10.1029/2018EO108991>, 2018.
946
947 Hill, D.F., Burakowski, E.A., Crumley, R.L., Keon, J., Hu, J.M., Arendt, A.A., Wikstrom Jones, K. and Wolken, G.J.: Converting
948 snow depth to snow water equivalent using climatological variables. *The Cryosphere*, 13(7), pp.1767-1784, <https://doi.org/10.5194/tc-13-1767-2019>, 2019.
949
950
951 Holko, L., Gorbachova, L. and Kostka, Z.: Snow hydrology in central Europe. *Geography Compass*, 5(4), pp.200-218,
952 <https://doi.org/10.1111/j.1749-8198.2011.00412.x>, 2011.
953
954 Homer, C., Dewitz, J., Yang, L., Jin, S., Danielson, P., Xian, G., Coulston, J., Herold, N., Wickham, J. and Megown, K.:
955 Completion of the 2011 National Land Cover Database for the conterminous United States—representing a decade of land cover
956 change information. *Photogrammetric Engineering & Remote Sensing*, 81(5), pp.345-354, [https://doi.org/10.1016/S0099-1112\(15\)30100-2](https://doi.org/10.1016/S0099-1112(15)30100-2), 2015.
957
958
959 Jonas, T., Marty, C. and Magnusson, J.: Estimating the snow water equivalent from snow depth measurements in the Swiss Alps.
960 *Journal of Hydrology*, 378(1-2), pp.161-167, <https://doi.org/10.1016/j.jhydrol.2009.09.021>, 2009.
961
962 Johnson, J.B.: A theory of pressure sensor performance in snow. *Hydrological Processes*, 18(1), pp.53-64,
963 <https://doi.org/10.1002/hyp.1310>, 2003.
964
965 Johnson, J.B. and Schaefer, G.L.: The influence of thermal, hydrologic, and snow deformation mechanisms on snow water
966 equivalent pressure sensor accuracy. *Hydrological Processes*, 16(18), pp.3529-3542, <https://doi.org/10.1002/hyp.1236>, 2002.
967

968 Kalnay, E., Kanamitsu, M., Kistler, R., Collins, W., Deaven, D., Gandin, L., Iredell, M., Saha, S., White, G., Woollen, J. and Zhu,
969 Y.: The NCEP/NCAR 40-year reanalysis project, *Bulletin of the American meteorological Society*, 77(3), pp.437-471,
970 [https://doi.org/10.1175/1520-0477\(1996\)077<0437:TNYRP>2.0.CO;2](https://doi.org/10.1175/1520-0477(1996)077<0437:TNYRP>2.0.CO;2), 1996.
971
972 Kalnay, E.: *Atmospheric modeling, data assimilation and predictability*. Cambridge university press, 2003.
973
974 Kapnick, S. and Hall, A.: Causes of recent changes in western North American snowpack. *Climate Dynamics*, 38(9-10), pp.1885-
975 1899, <https://doi.org/10.1007/s00382-011-1089-y>, 2012.
976
977 King, J.M., Cabrera, A.R. and Kelly, R.E.: The Snowtweets Project: Communicating snow depth measurements from specialists
978 and non-specialists via mobile communication technologies and social networks. AGU Fall Meeting Abstracts, Bibcode:
979 2009AGUFMED11A0562K, 2009.
980
981 Lader, R., Bhatt, U.S., Walsh, J.E., Rupp, T.S. and Bieniek, P.A.: Two-meter temperature and precipitation from atmospheric
982 reanalysis evaluated for Alaska, *Journal of Applied Meteorology and Climatology*, 55(4), pp.901-922,
983 <https://doi.org/10.1175/JAMC-D-15-0162.1>, 2016.
984
985 Lehning, M., Bartelt, P., Brown, B., Russi, T., Stöckli, U. and Zimmerli, M. SNOWPACK model calculations for avalanche
986 warning based upon a new network of weather and snow stations. *Cold Regions Science and Technology*, 30(1-3), pp.145-157,
987 [https://doi.org/10.1016/S0165-232X\(99\)00022-1](https://doi.org/10.1016/S0165-232X(99)00022-1), 1999.
988
989 Lehning, M., Völksch, I., Gustafsson, D., Nguyen, T.A., Stähli, M. and Zappa, MALPINE3D: a detailed model of mountain surface
990 processes and its application to snow hydrology. *Hydrological Processes: An International Journal*, 20(10), pp.2111-2128,
991 <https://doi.org/10.1002/hyp.6204>, 2006.
992
993 Li, D., Wigmore, O., Durand, M.T., Vander-Jagt, B., Margulis, S.A., Molotch, N.P. and Bales, R.C.: Potential of Balloon
994 Photogrammetry for Spatially Continuous Snow Depth Measurements. *IEEE Geoscience and Remote Sensing Letters*,
995 <https://doi.org/10.1109/LGRS.2019.2953481>, 2019.
996
997 Liston, G.E. and Elder, K.: A distributed snow-evolution modeling system (SnowModel), *Journal of Hydrometeorology*, 7(6),
998 pp.1259-1276, <https://doi.org/10.1175/JHM548.1>, 2006a.
999
1000 Liston, G.E. and Elder, K.: A meteorological distribution system for high-resolution terrestrial modeling (MicroMet), *Journal of*
1001 *Hydrometeorology*, 7(2), pp.217-234, <https://doi.org/10.1175/JHM486.1>, 2006b.
1002
1003 Liston, G.E., Haehnel, R.B., Sturm, M., Hiemstra, C.A., Berezovskaya, S. and Tabler, R.D.: Simulating complex snow distributions
1004 in windy environments using SnowTran-3D. *Journal of Glaciology*, 53(181), pp.241-256,
1005 <https://doi.org/10.3189/172756507782202865>, 2007.
1006
1007 Liston, G.E. and Hiemstra, C.A.: A simple data assimilation system for complex snow distributions (SnowAssim). *Journal of*
1008 *Hydrometeorology*, 9(5), pp.989-1004, <https://doi.org/10.1175/2008JHM871.1>, 2008.
1009

1010 Liston, G.E. and Hiemstra, C.A.: The changing cryosphere: Pan-Arctic snow trends (1979–2009). *Journal of Climate*, 24(21),
1011 pp.5691-5712, <https://doi.org/10.1175/JCLI-D-11-00081.1>, 2011.

1012

1013 López-Moreno, J.I., Fassnacht, S.R., Heath, J.T., Musselman, K.N., Revuelto, J., Latron, J., Morán-Tejeda, E. and Jonas, T.: Small
1014 scale spatial variability of snow density and depth over complex alpine terrain: Implications for estimating snow water equivalent.
1015 *Advances in water resources*, 55, pp.40-52, <https://doi.org/10.1016/j.advwatres.2012.08.010>, 2013.

1016

1017 Lowry, C.S. and Fienen, M.N.: CrowdHydrology: crowdsourcing hydrologic data and engaging citizen scientists. *GroundWater*,
1018 51(1), pp.151-156, <https://doi.org/10.1111/j.1745-6584.2012.00956.x>, 2013.

1019

1020 Luce, C.H., Tarboton, D.G. and Cooley, K.R.: The influence of the spatial distribution of snow on basin-averaged snowmelt.
1021 *Hydrological Processes*, 12(10-11), pp.1671-1683, [https://doi.org/10.1002/\(SICI\)1099-1085\(199808/09\)12:10/11<1671::AID-
1022 HYP688>3.0.CO;2-N](https://doi.org/10.1002/(SICI)1099-1085(199808/09)12:10/11<1671::AID-), 1998.

1023

1024 Luoju, K., Pulliainen, J., Takala, M., Derksen, C., Rott, H., Nagler, T., Solberg, R., Wiesmann, A., Metsamaki, S., Malnes, E. and
1025 Bojkov, B.: Investigating the feasibility of the GlobSnow snow water equivalent data for climate research purposes. In 2010 IEEE
1026 International Geoscience and Remote Sensing Symposium (pp. 4851-4853), IEEE,
1027 <https://doi.org/10.1109/IGARSS.2010.5741987>, 2010.

1028

1029 Magnusson, J., Gustafsson, D., Hüsler, F. and Jonas, T.: Assimilation of point SWE data into a distributed snow cover model
1030 comparing two contrasting methods. *Water resources research*, 50(10), pp.7816-7835, <https://doi.org/10.1002/2014WR015302>,
1031 2014.

1032

1033 Magnusson, J., Winstral, A., Stordal, A.S., Essery, R. and Jonas, T.: Improving physically based snow simulations by assimilating
1034 snow depths using the particle filter. *Water Resources Research*, 53(2), pp.1125-1143, <https://doi.org/10.1002/2016WR019092>,
1035 2017.

1036

1037 Malik, M.J., van der Velde, R., Vekerdy, Z. and Su, Z.: Assimilation of satellite-observed snow albedo in a land surface model.
1038 *Journal of hydrometeorology*, 13(3), pp.1119-1130, <https://doi.org/10.1175/JHM-D-11-0125.1>, 2012.

1039

1040 Mankin, J.S., Viviroli, D., Singh, D., Hoekstra, A.Y. and Diffenbaugh, N.S.: The potential for snow to supply human water demand
1041 in the present and future. *Environmental Research Letters*, 10(11), p.114016, <https://doi.org/10.1088/1748-9326/10/11/114016>,
1042 2015.

1043

1044 Margulis, S.A., Giroto, M., Cortés, G. and Durand, M.: A particle batch smoother approach to snow water equivalent estimation.
1045 *Journal of Hydrometeorology*, 16(4), pp.1752-1772, <https://doi.org/10.1175/JHM-D-14-0177.1>, 2015.

1046

1047 Marks, D., Domingo, J., Susong, D., Link, T. and Garen, D.: A spatially distributed energy balance snowmelt model for application
1048 in mountain basins, *Hydrological Processes*, 13(12-13), pp.1935-1959, [https://doi.org/10.1002/\(SICI\)1099-
1049 1085\(199909\)13:12/13<1935::AID-HYP868>3.0.CO;2-C](https://doi.org/10.1002/(SICI)1099-), 1999.

1050

1051 Massey Jr, F.J.:The Kolmogorov-Smirnov test for goodness of fit. *Journal of the American statistical Association*, 46(253), pp.68-
1052 78, 1951.
1053
1054 McCreight, J.L., Small, E.E. and Larson, K.M.: Snow depth, density, and SWE estimates derived from GPS reflection data:
1055 Validation in the western US. *Water Resources Research*, 50(8), pp.6892-6909, <https://doi.org/10.1002/2014WR015561>, 2014.
1056
1057 McGuire, M., Wood, A.W., Hamlet, A.F. and Lettenmaier, D.P.: Use of satellite data for streamflow and reservoir storage forecasts
1058 in the Snake River Basin. *Journal of Water Resources Planning and Management*, 132(2), pp.97-110,
1059 [https://doi.org/10.1061/\(ASCE\)0733-9496\(2006\)132:2\(97\)](https://doi.org/10.1061/(ASCE)0733-9496(2006)132:2(97)) 2006.
1060
1061 McLaughlin, D.: An integrated approach to hydrologic data assimilation: interpolation, smoothing, and filtering. *Advances in*
1062 *Water Resources*, 25(8), pp.1275-1286, [https://doi.org/10.1016/S0309-1708\(02\)00055-6](https://doi.org/10.1016/S0309-1708(02)00055-6), 2002.
1063
1064 McKinley, D.C., Miller-Rushing, A.J., Ballard, H.L., Bonney, R., Brown, H., Cook-Patton, S.C., Evans, D.M., French, R.A.,
1065 Parrish, J.K., Phillips, T.B. and Ryan, S.F.: Citizen science can improve conservation science, natural resource management, and
1066 environmental protection. *Biological Conservation*, 208, pp.15-28, <https://doi.org/10.1016/j.biocon.2016.05.015>, 2017.
1067
1068 McMillan, H.K., Hreinsson, E.Ö., Clark, M.P., Singh, S.K., Zammit, C. and Uddstrom, M.J.: Operational hydrological data
1069 assimilation with the recursive ensemble Kalman filter. *Hydrology and Earth System Sciences*, 17(1), pp.21-38,
1070 <https://doi.org/10.5194/hess-17-21-2013>, 2013.
1071
1072 Mernild, S.H., Liston, G.E., Hasholt, B. and Knudsen, N.T.: Snow distribution and melt modeling for Mittivakkat Glacier,
1073 Ammassalik Island, southeast Greenland. *Journal of Hydrometeorology*, 7(4), pp.808-824, <https://doi.org/10.1175/JHM522.1>,
1074 2006.
1075
1076 Mernild, S.H., Liston, G.E., Hiemstra, C.A., Malmros, J.K., Yde, J.C. and McPhee, J.: The Andes Cordillera. Part I: snow
1077 distribution, properties, and trends (1979–2014), *International Journal of Climatology*, 37(4), pp.1680-1698,
1078 <https://doi.org/10.1002/joc.4804>, 2017a.
1079
1080 Mernild, S.H., Liston, G.E., Hiemstra, C.A., Yde, J.C., McPhee, J. and Malmros, J.K.: The Andes Cordillera. Part II: Rio Olivares
1081 Basin snow conditions (1979–2014), central Chile, *International Journal of Climatology*, 37(4), pp.1699-1715,
1082 <https://doi.org/10.1002/joc.4828>, 2017b.
1083
1084 Mesinger, F., DiMego, G., Kalnay, E., Mitchell, K., Shafran, P.C., Ebisuzaki, W., Jović, D., Woollen, J., Rogers, E., Berbery, E.H.
1085 and Ek, M.B.: North American regional reanalysis, *Bulletin of the American Meteorological Society*, 87(3), pp.343-360,
1086 <https://doi.org/10.1175/BAMS-87-3-343>, 2006.
1087
1088 Molotch, N.P. and Bales, R.C.: Scaling snow observations from the point to the grid element: Implications for observation network
1089 design. *Water Resources Research*, 41(11), <https://doi.org/10.1029/2005WR004229>, 2005a.
1090

1091 Molotch, N.P., Colee, M.T., Bales, R.C. and Dozier, J.: Estimating the spatial distribution of snow water equivalent in an alpine
1092 basin using binary regression tree models: the impact of digital elevation data and independent variable selection. *Hydrological*
1093 *Processes: An International Journal*, 19(7), pp.1459-1479, <https://doi.org/10.1002/hyp.5586>, 2005b.
1094
1095 Mote, P.W., Li, S., Lettenmaier, D.P., Xiao, M. and Engel, R.: Dramatic declines in snowpack in the western US. *Npj Climate and*
1096 *Atmospheric Science*, 1(1), pp.1-6, <https://doi.org/10.1038/s41612-018-0012-1>, 2018.
1097
1098 NOHRSC: Snow Data Assimilation System (SNODAS) Data Products at NSIDC, Version 1. Boulder, Colorado USA. NSIDC:
1099 National Snow and Ice Data Center. doi: <https://doi.org/10.7265/N5TB14TC>, 2004.
1100
1101 Pagano, T., Garen, D., Perkins, T., and Pasteris, P.: Daily updating of operational statistical seasonal water supply forecasts for the
1102 western U.S., *J. Am. Water Resour. As.*, 45, 767–778, <https://doi.org/10.1111/j.1752-1688.2009.00321.x>, 2009.
1103
1104 Painter, T.H., Berisford, D.F., Boardman, J.W., Bormann, K.J., Deems, J.S., Gehrke, F., Hedrick, A., Joyce, M., Laidlaw, R.,
1105 Marks, D. and Mattmann, C.: The Airborne Snow Observatory: Fusion of scanning lidar, imaging spectrometer, and physically-
1106 based modeling for mapping snow water equivalent and snow albedo. *Remote Sensing of Environment*, 184, pp.139-152,
1107 <https://doi.org/10.1016/j.rse.2016.06.018>, 2016.
1108
1109 Park, S.K. and Xu, L. eds.: Data assimilation for atmospheric, oceanic and hydrologic applications (Vol. 2). Springer Science &
1110 Business Media, 2013.
1111
1112 Pistocchi, A.: Simple estimation of snow density in an Alpine region. *Journal of Hydrology: Regional Studies*, 6, pp.82-89,
1113 <https://doi.org/10.1016/j.ejrh.2016.03.004>, 2016.
1114
1115 Pomeroy, J.W., Gray, D.M. and Landine, P.G. The prairie blowing snow model: characteristics, validation, operation. *Journal of*
1116 *Hydrology*, 144(1-4), pp.165-192, [https://doi.org/10.1016/0022-1694\(93\)90171-5](https://doi.org/10.1016/0022-1694(93)90171-5), 1993.
1117
1118 Rabier, F.: Overview of global data assimilation developments in numerical weather-prediction centres. *Quarterly Journal of the*
1119 *Royal Meteorological Society: A journal of the atmospheric sciences, applied meteorology and physical oceanography*, 131(613),
1120 pp.3215-3233, <https://doi.org/10.1256/qj.05.129>, 2005.
1121
1122 Reges, H.W., Doesken, N., Turner, J., Newman, N., Bergantino, A. and Schwalbe, Z.: COCORAHs: The evolution and
1123 accomplishments of a volunteer rain gauge network. *Bulletin of the American Meteorological Society*, 97(10), pp.1831-1846,
1124 <https://doi.org/10.1175/BAMS-D-14-00213.1>, 2016.
1125
1126 Reichle, R.H., McLaughlin, D.B. and Entekhabi, D.: Hydrologic data assimilation with the ensemble Kalman filter. *Monthly*
1127 *Weather Review*, 130(1), pp.103-114, [https://doi.org/10.1175/1520-0493\(2002\)130<0103:HDAWTE>2.0.CO;2](https://doi.org/10.1175/1520-0493(2002)130<0103:HDAWTE>2.0.CO;2), 2002.
1128
1129 Reichle, R.H.: Data assimilation methods in the Earth sciences. *Advances in water resources*, 31(11), pp.1411-1418,
1130 <https://doi.org/10.1016/j.advwatres.2008.01.001/>, 2008.
1131

1132 Rice, R. and Bales, R.C.: Embedded-sensor network design for snow cover measurements around snow pillow and snow course
1133 sites in the Sierra Nevada of California. *Water Resources Research*, 46(3), <https://doi.org/10.1029/2008WR007318>, 2010.
1134
1135 Riemann, R., Wilson, B.T., Lister, A. and Parks, S.: An effective assessment protocol for continuous geospatial datasets of forest
1136 characteristics using USFS Forest Inventory and Analysis (FIA) data. *Remote Sensing of Environment*, 114(10), pp.2337-2352,
1137 <https://doi.org/10.1016/j.rse.2010.05.010>, 2010.
1138
1139 Rivington, M., Matthews, K.B., Bellocchi, G. and Buchan, K.: Evaluating uncertainty introduced to process-based simulation
1140 model estimates by alternative sources of meteorological data. *Agricultural Systems*, 88(2-3), pp.451-471,
1141 <https://doi.org/10.1016/j.agsy.2005.07.004>, 2006.
1142
1143 Saha, S., Moorthi, S., Pan, H.L., Wu, X., Wang, J., Nadiga, S., Tripp, P., Kistler, R., Woollen, J., Behringer, D. and Liu, H.: The
1144 NCEP climate forecast system reanalysis. *Bulletin of the American Meteorological Society*, 91(8), pp.1015-1058,
1145 <https://doi.org/10.1175/2010BAMS3001.1>, 2010.
1146
1147 Saha, S., Moorthi, S., Wu, X., Wang, J., Nadiga, S., Tripp, P., Behringer, D., Hou, Y.T., Chuang, H.Y., Iredell, M. and Ek, M.:
1148 The NCEP climate forecast system version 2. *Journal of Climate*, 27(6), pp.2185-2208, <https://doi.org/10.1175/JCLI-D-12-00823.1>, 2014.
1149
1150
1151 Schmucki, E., Marty, C., Fierz, C. and Lehning, M.: Evaluation of modelled snow depth and snow water equivalent at three
1152 contrasting sites in Switzerland using SNOWPACK simulations driven by different meteorological data input. *Cold Regions
1153 Science and Technology*, 99, pp.27-37, <https://doi.org/10.1016/j.coldregions.2013.12.004>, 2014.
1154
1155 Schaefer, M. and Woodyer, T.: Assessing absolute and relative accuracy of recreation-grade and mobile phone GNSS devices: a
1156 method for informing device choice. *Area*, 47(2), pp.185-196, <https://doi.org/10.1111/area.12172>, 2015.
1157
1158 Schlögl, S., Marty, C., Bavay, M. and Lehning, M.: Sensitivity of Alpine3D modeled snow cover to modifications in DEM
1159 resolution, station coverage and meteorological input quantities. *Environmental modelling & software*, 83, pp.387-396,
1160 <https://doi.org/10.1016/j.envsoft.2016.02.017>, 2016.
1161
1162 Schneider, C., Laizé, C.L.R., Acreman, M.C. and Flörke, M.: How will climate change modify river flow regimes in Europe?.
1163 *Hydrology and Earth System Sciences*, 17(1), pp.325-339, <https://doi.org/10.5194/hess-17-325-2013>, 2013.
1164
1165 Seibert, J., Strobl, B., Etter, S., Hummer, P. and van Meerveld, H.J.: Virtual staff gauges for crowd-based stream level observations.
1166 *Frontiers in Earth Science - Hydrosphere*, 7, p.70, <https://doi.org/10.3389/feart.2019.00070>, 2019.
1167
1168 Serreze, M.C., Clark, M.P., Armstrong, R.L., McGinnis, D.A. and Pulwarty, R.S.: Characteristics of the western United States
1169 snowpack from snowpack telemetry (SNOTEL) data. *Water Resources Research*, 35(7), pp.2145-2160,
1170 <https://doi.org/10.1029/1999WR900090>, 1999.
1171
1172 Shulski, M. and Wendler, G.: *The climate of Alaska*. University of Alaska Press, 2007.
1173

1174 Silvertown, J.: A new dawn for citizen science. *Trends in ecology & evolution*, 24(9), pp.467-471,
1175 <https://doi.org/10.1016/j.tree.2009.03.017>, 2009.
1176

1177 Sturm, M., Holmgren, J. and Liston, G.E.: A seasonal snow cover classification system for local to global applications. *Journal of*
1178 *Climate*, 8(5), pp.1261-1283, [https://doi.org/10.1175/1520-0442\(1995\)008<1261:ASSCCS>2.0.CO;2](https://doi.org/10.1175/1520-0442(1995)008<1261:ASSCCS>2.0.CO;2), 1995.
1179

1180 Sturm, M., Taras B., Liston G., Derksen, C., Jonas T., and Lea, J.: Estimating Snow Water Equivalent Using Snow Depth Data
1181 and Climate Classes. *Journal of Hydrometeorology* 11 (6): 1380–94. <https://doi.org/10.1175/2010JHM1202.1>, 2010a.
1182

1183 Sturm, M. and Wagner, A.M.: Using repeated patterns in snow distribution modeling: An Arctic example. *Water Resources*
1184 *Research*, 46(12), <https://doi.org/10.1029/2010WR009434>, 2010b.
1185

1186 Sturm, M.: White water: Fifty years of snow research in WRR and the outlook for the future. *Water Resources Research*, 51(7),
1187 pp.4948-4965, <https://doi.org/10.1002/2015WR017242>, 2015.
1188

1189 Trujillo, E., Molotch, N.P., Goulden, M.L., Kelly, A.E. and Bales, R.C.: Elevation-dependent influence of snow accumulation on
1190 forest greening. *Nature Geoscience*, 5(10), pp.705-709, <https://doi.org/10.1038/ngeo1571>, 2012.
1191

1192 van Meerveld, H. J. I., Vis, M. J. P., and Seibert, J.: Information content of stream level class data for hydrological model
1193 calibration, *Hydrol. Earth Syst. Sci.*, 21, 4895-4905, <https://doi.org/10.5194/hess-21-4895-2017>, 2017.
1194

1195 Viviroli, D., Dürr, H.H., Messerli, B., Meybeck, M. and Weingartner, R.: Mountains of the world, water towers for humanity:
1196 Typology, mapping, and global significance. *Water resources research*, 43(7), <https://doi.org/10.1029/2006WR005653>, 2007.
1197

1198 Wagner, W.: Investigating the snow climate of Turnagain Pass, Alaska. In *Proceedings of the International Snow Science*
1199 *Workshop*, Anchorage, AK (pp. 913-917), 2012.
1200

1201 Wiggins, A. and Crowston, K.: From conservation to crowdsourcing: A typology of citizen science. In *2011 44th Hawaii*
1202 *international conference on system sciences* (pp. 1-10). IEEE, <https://doi.org/10.1109/HICSS.2011.207>, 2011.
1203

1204 Wrzesien, M.L., Durand, M.T., Pavelsky, T.M., Howat, I.M., Margulis, S.A. and Huning, L.S.: Comparison of methods to estimate
1205 snow water equivalent at the mountain range scale: a case study of the California Sierra Nevada. *Journal of Hydrometeorology*,
1206 18(4), pp.1101-1119, <https://doi.org/10.1175/JHM-D-16-0246.1>, 2017.
1207

1208 Yeeles, A.: Citizen snow-scientists trek into the back country. *Nature Climate Change*, 8(11), p.944,
1209 <https://doi.org/10.1038/s41558-018-0329-0>, 2018.
1210

1211 Young, J.C., Pettit, E., Arendt, A., Hood, E., Liston, G.E. and Beamer, J.: A changing hydrological regime: Trends in magnitude
1212 and timing of glacier ice melt and glacier runoff in a high latitude coastal watershed. *Water Resources Research*,
1213 p.e2020WR027404, 2020.